

Sensor and Simulation Notes

Note 227

September 1977

Modes on a Finite-Width Parallel-Plate Simulator  
III. Numerical Results for Modes on Wide Plates

Lennart Marin  
G.C. Lewis, Jr.

Dikewood Corporation, Westwood Research Branch  
Los Angeles, California

Abstract

Numerical results are presented for (1) the transverse wave numbers, (2) the frequency variations of the longitudinal propagation and attenuation constants, and (3) the field distributions of the higher-order modes on two parallel wide plates. It is found that the least attenuated modes are the antisymmetric TE modes.

CLEARED  
FOR PUBLIC RELEASE  
FL/FA 31 DEC 96

ACKNOWLEDGEMENT

Thanks go to Drs. C.E. Baum, J.P. Castillo, and K.C. Chen of the Air Force Weapons Laboratory for many enlightening discussions.

01 96-1072

## SECTION I

### INTRODUCTION

The working volume of most bounded-wave simulators consists of the forward region between two parallel plates (figure 1). Test objects such as aircraft and missiles are placed in the simulators' working volume during tests. The electromagnetic field in the parallel-plate region can be decomposed into a TEM mode, higher-order TE and TM modes and a part due to the continuous spectrum. The TEM modes on two finite-width, parallel plates have been investigated extensively (refs. 1, 2, and 3). In all these references the method of conformal mapping is used, the actual conformal transformation being that derived in ref. 4.

The properties of the higher-order modes on two finite-width parallel plates have been investigated in some limiting cases. When the width of the plates is small compared to the distance separating the plates then it was found in ref. 5 that the TE modes are more attenuated as they propagate along the simulator than are the TM modes. The field lines and the field distributions of the fundamental TM modes are also investigated in this reference.

A transverse-resonance method of calculating the propagation constants for the higher-order modes on a finite-width parallel-plate waveguide is given by Weinstein (ref. 6). This method is used in ref. 7 to find the propagation constants for the fundamental higher-order modes when the width of the plates is larger than the distance separating the plates.

The method of Wiener and Hopf was used in ref. 8 to derive Fredholm integral equations of the second kind for the electromagnetic field on two parallel, finite-width plates. These integral equations were then used to find approximate analytical expressions for the propagation constants and field distributions of the higher-order modes on two wide plates. In the wide-plate case it was found in ref. 8 that the TE modes are the least attenuated modes as they propagate along the simulator.

In this report we will use the results of ref. 8 to tabulate and graphically display the following quantities: (i) the transverse (complex) wavenumbers of

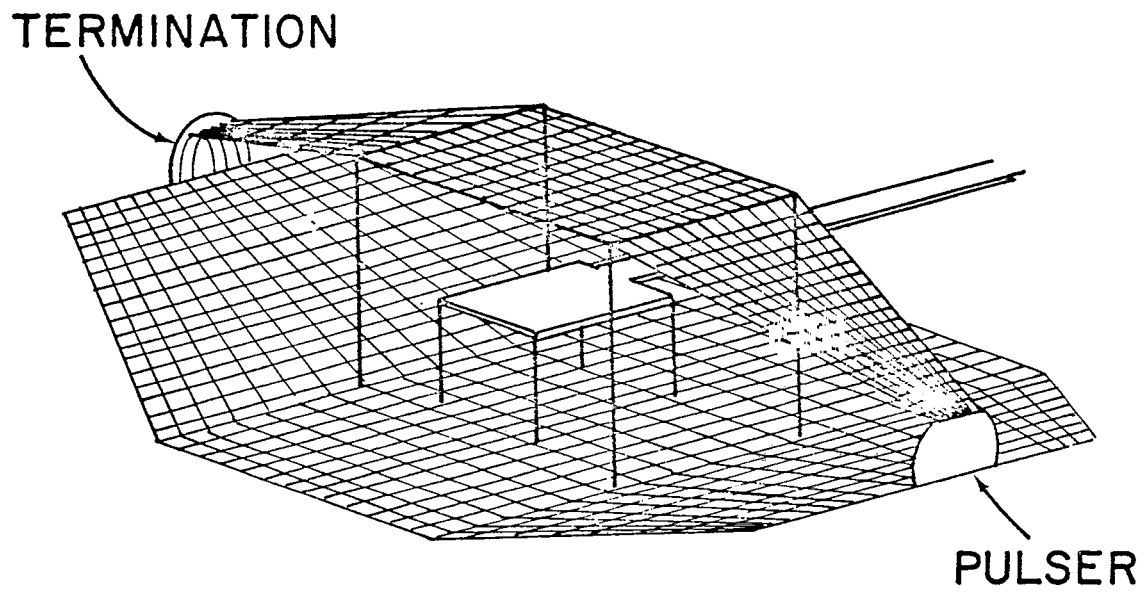
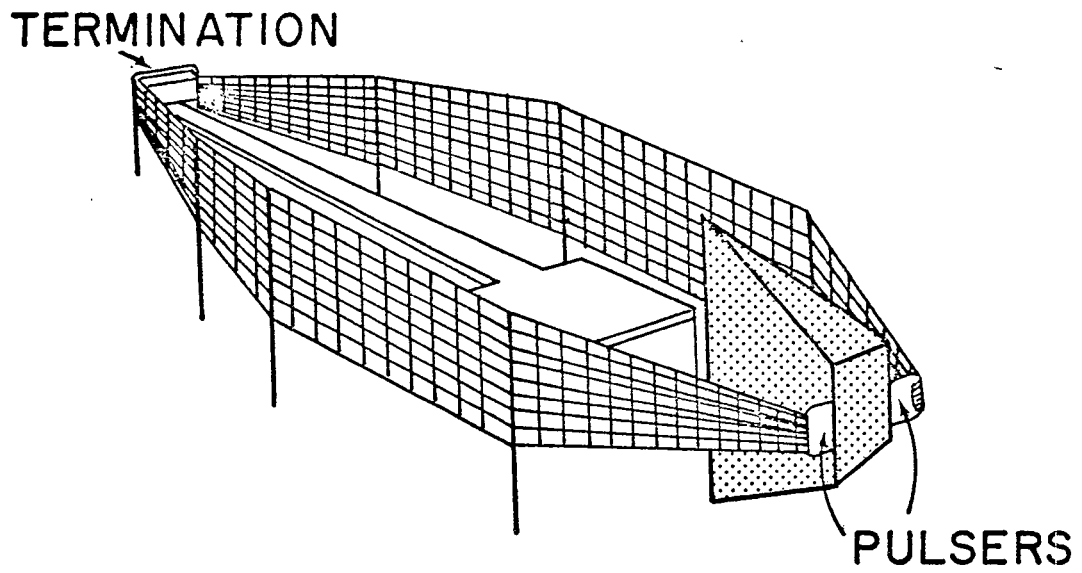


Figure 1. Schematic drawings of bounded-wave simulators.

the higher-order TE and TM modes, (ii) the frequency variation of the longitudinal propagation and attenuation constants of the most important higher-order modes, (iii) the field strengths of the fundamental higher-order modes, and (iv) the field lines of these modes.

## SECTION II

### TRANSVERSE COMPLEX WAVE NUMBERS

In a previous report (ref. 8) modes other than the TEM modes on two parallel wide plates are investigated. It is found that the most natural decomposition of these higher-order modes is to use (1) transverse electric modes (H-modes) and transverse magnetic modes (E-modes), (2) symmetric and antisymmetric modes, referring to the symmetry of the electromagnetic field in the direction perpendicular to the plates (or y-direction, figure 2), and (3) even and odd modes, referring to the symmetry of the electromagnetic field in the transverse direction parallel to the plates (or x-direction).

Let us pause for a moment and discuss this decomposition. The notation antisymmetric is used for those modes where the  $E_x$ ,  $E_z$ , and  $H_y$  components vanish at the  $y=0$  plane. Thus, the antisymmetric modes on two parallel plates coincide with the modes of one plate above and parallel to a ground plane (figure 3). Furthermore, the antisymmetric modes are the only modes excited in the simulator at the top of figure 1. The notation odd is used for those modes where the  $E_y$ ,  $E_z$ , and  $H_x$  components vanish at the  $x=0$  plane. For a general discussion of symmetry properties of the electromagnetic field we refer to ref. 9.

It is found in ref. 8 that the antisymmetric TE modes are of main interest, the reason being that these modes have the smallest attenuation constant as they propagate along the plates. The second most important modes are the symmetric TE and TM modes. The antisymmetric TM modes are the most highly damped ones. In this section we will therefore scrutinize the transverse propagation constants of (1) the even, antisymmetric TE modes, (2) the odd, antisymmetric TE modes, (3) the even, symmetric TE modes, (4) the odd, symmetric TE modes, (5) the even, symmetric TM modes, and (6) the odd, symmetric TM modes.

#### *1. Mathematical Expressions for the Transverse Complex Wave Numbers*

The transcendental equations and their asymptotic solutions from which the transverse wave numbers are obtained are presented in ref. 8. For the sake of completeness we list here the transcendental equations together with their

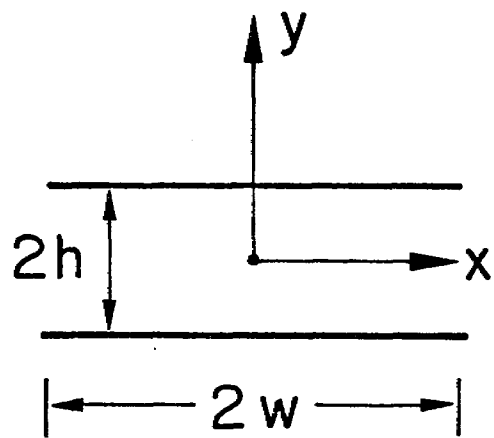
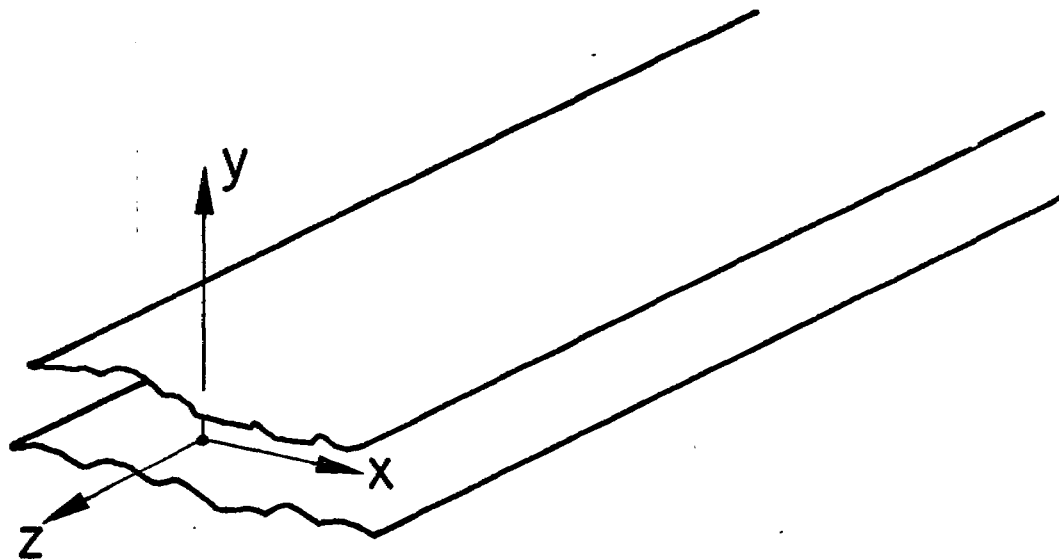


Figure 2. Two, finite-width, parallel plates.

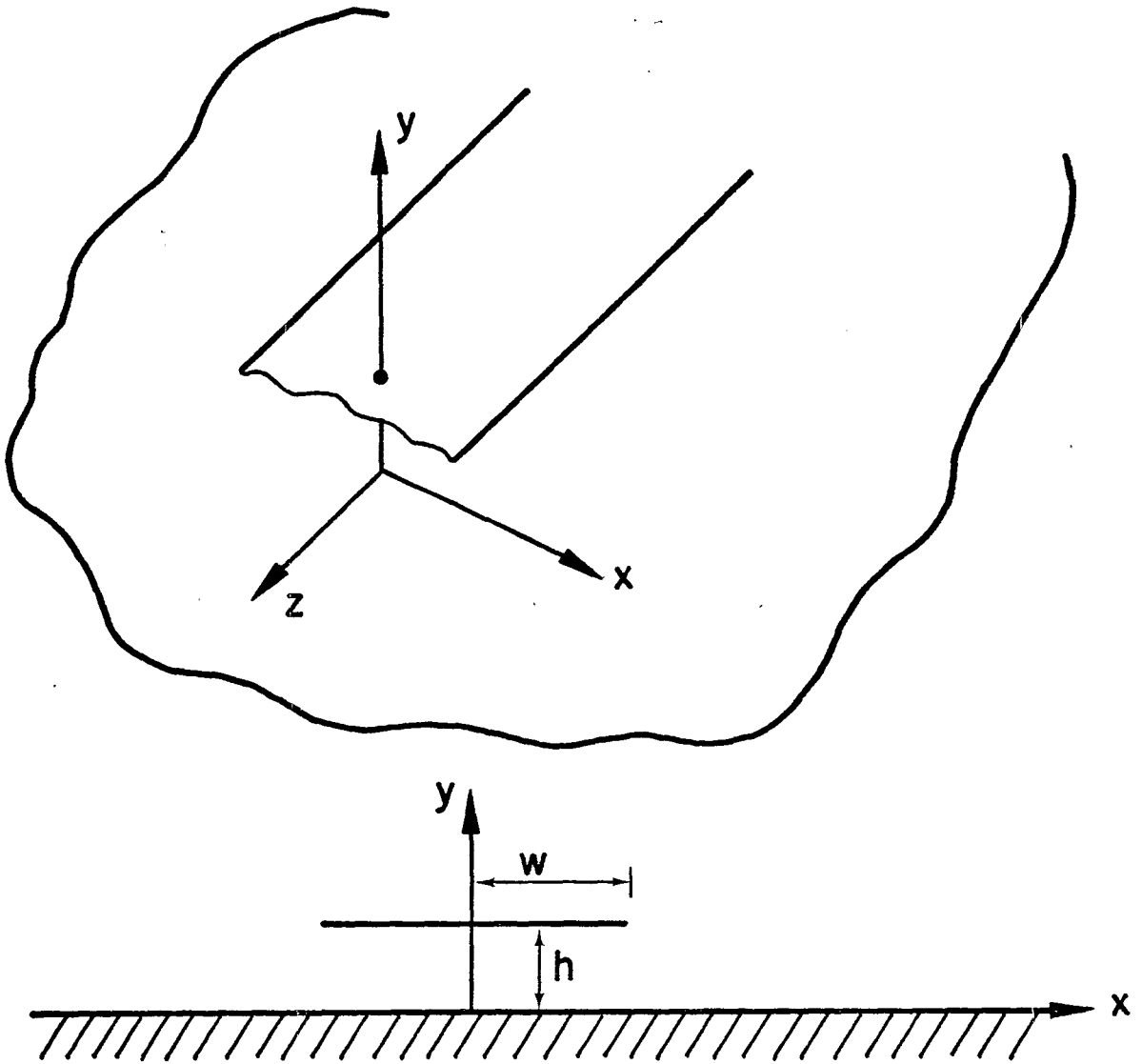


Figure 3. A finite-width plate above a ground plane.

asymptotic solutions when  $|pw| \gg 1$  for the four types of modes listed previously. The symbol  $p$  represents the transverse complex wave number and the symbol  $w$  denotes the half-width of the plates. Superscripts ' and " pretypify TM and TE, respectively. Superscript  $e$  indicates even whereas superscript  $o$  indicates odd. Furthermore, subscript  $s$  stands for symmetric and subscript  $a$  stands for antisymmetric. The quantity  $n$  portrays the integer order of a particular mode.

A. Even, Antisymmetric TE Modes

$$1 - \exp \left\{ 2pw + \frac{2}{\pi} ph \left[ \ln \left( \frac{2\pi}{ph} \right) - \gamma + 1 \right] \right\} - h \sqrt{\frac{p}{w\pi}} = 0$$

$$p_{a,n}^{''e} w = i\pi n \left\{ 1 - \frac{h}{\pi w} \left[ \ln \left( \frac{2\pi w}{nh} \right) - \gamma + 1 - \frac{1}{2\sqrt{2n}} \right] \right\} \quad (1)$$

$$- \pi n \frac{h}{w} \left[ \frac{1}{2} + \frac{1}{2\pi\sqrt{2n}} \right], \quad \frac{h}{w} \ll 1$$

B. Odd, Antisymmetric TE Modes

$$1 + \exp \left\{ 2pw + \frac{2}{\pi} ph \left[ \ln \left( \frac{2\pi}{ph} \right) - \gamma + 1 \right] \right\} - h \sqrt{\frac{p}{w\pi}} = 0$$

$$p_{a,n}^{''o} w = i\pi \left( n - \frac{1}{2} \right) \left\{ 1 - \frac{h}{\pi w} \left[ \ln \left( \frac{4\pi w}{(2n-1)h} \right) - \gamma + 1 - \frac{1}{2\sqrt{2n-1}} \right] \right\} \quad (2)$$

$$- \pi \left( n - \frac{1}{2} \right) \frac{h}{w} \left[ \frac{1}{2} + \frac{1}{2\pi\sqrt{2n-1}} \right], \quad \frac{h}{w} \ll 1$$

C. Even, Symmetric TE Modes

$$2\sqrt{\pi} \sqrt{pw} \exp(2pw) + 1 = 0 \quad (3)$$

$$p_{s,n}^{''e} w = \left( n + \frac{3}{8} \right) \pi i - \frac{1}{4} \ln(4\pi^2 n)$$

D. Odd, Symmetric TE Modes

$$2\sqrt{\pi} \sqrt{pw} \exp(2pw) - 1 = 0 \quad (4)$$

$$p''_{s,n} w = \left(n - \frac{1}{8}\right) \pi i - \frac{1}{4} \ln(4\pi^2 n)$$

E. Even, Symmetric TM Modes

$$16\sqrt{\pi} (pw)^{3/2} \exp(2pw) - 1 = 0 \quad (5)$$

$$p'_{s,n} w = \left(n - \frac{3}{8}\right) \pi i - \frac{1}{4} \ln(256 \pi^4 n^3) + 0(n^{-1} \ln n)$$

F. Odd, Symmetric TM Modes

$$16\sqrt{\pi} (pw)^{3/2} \exp(2pw) + 1 = 0 \quad (6)$$

$$p'_{s,n} w = \left(n + \frac{1}{8}\right) \pi i - \frac{1}{4} \ln(256 \pi^4 n^3) + 0(n^{-1} \ln n)$$

2. *Calculated Values of the Transverse Complex Wave Numbers*

The transcendental equations (1) through (6) were solved numerically and the results of these calculations are shown in figures 4 and 5 and table 1.

We observe from these results that the absolute value of the real part of  $p''_{a,n}$  is much smaller than those of  $p''_{s,n}$  and  $p'_{s,n}$ . In the next section we will see how this fact implies that the antisymmetric TE modes are less attenuated as they propagate along the simulator than are the symmetric TE and TM modes. We also mention that the roots of (1) through (6) occur in complex conjugate pairs. The only ones included in figure 4 and 5 and table 1 are those in the second quadrant.

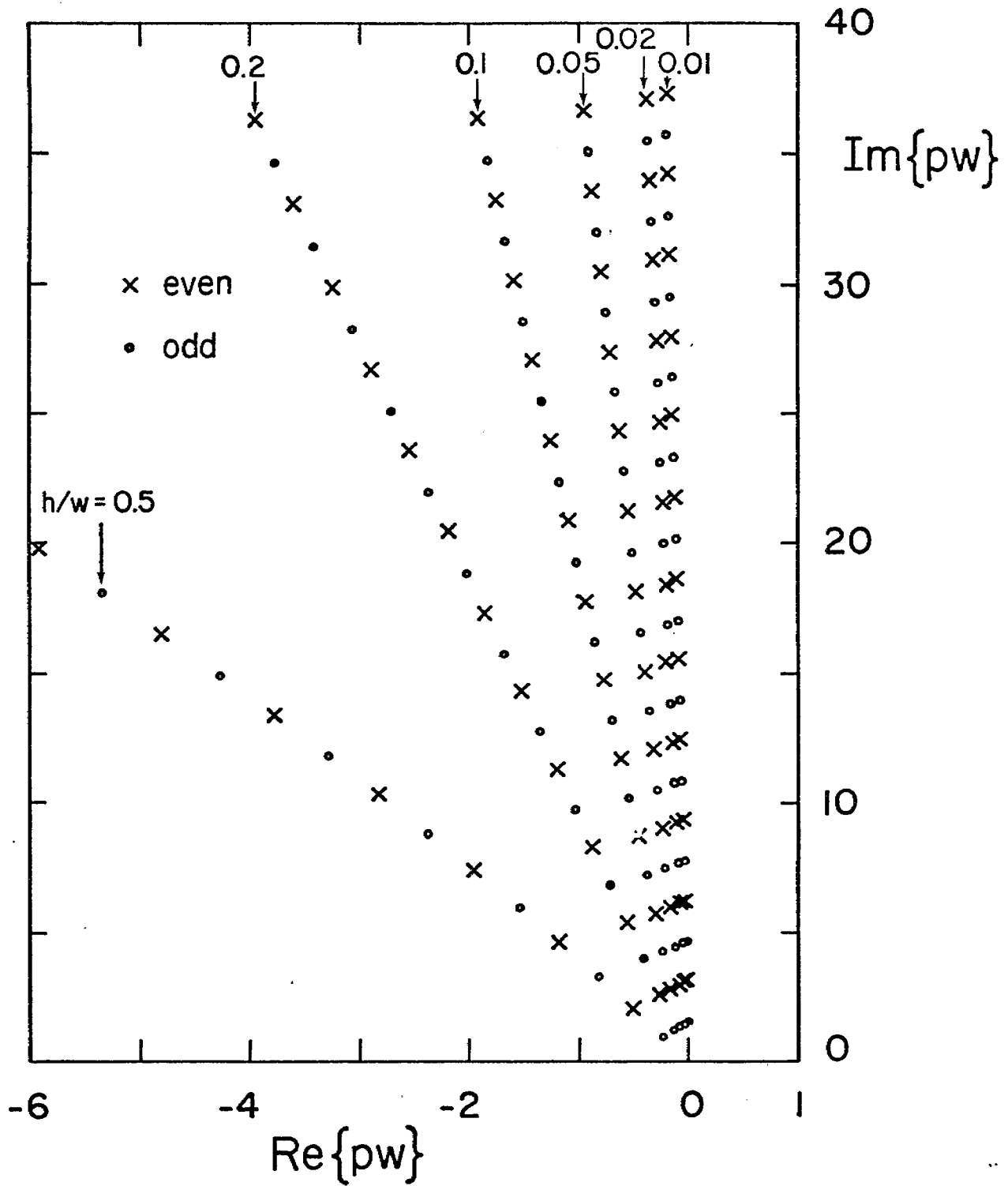


Figure 4. The transverse propagation constants for the antisymmetric TE modes  $(p''_{a,n})$ .

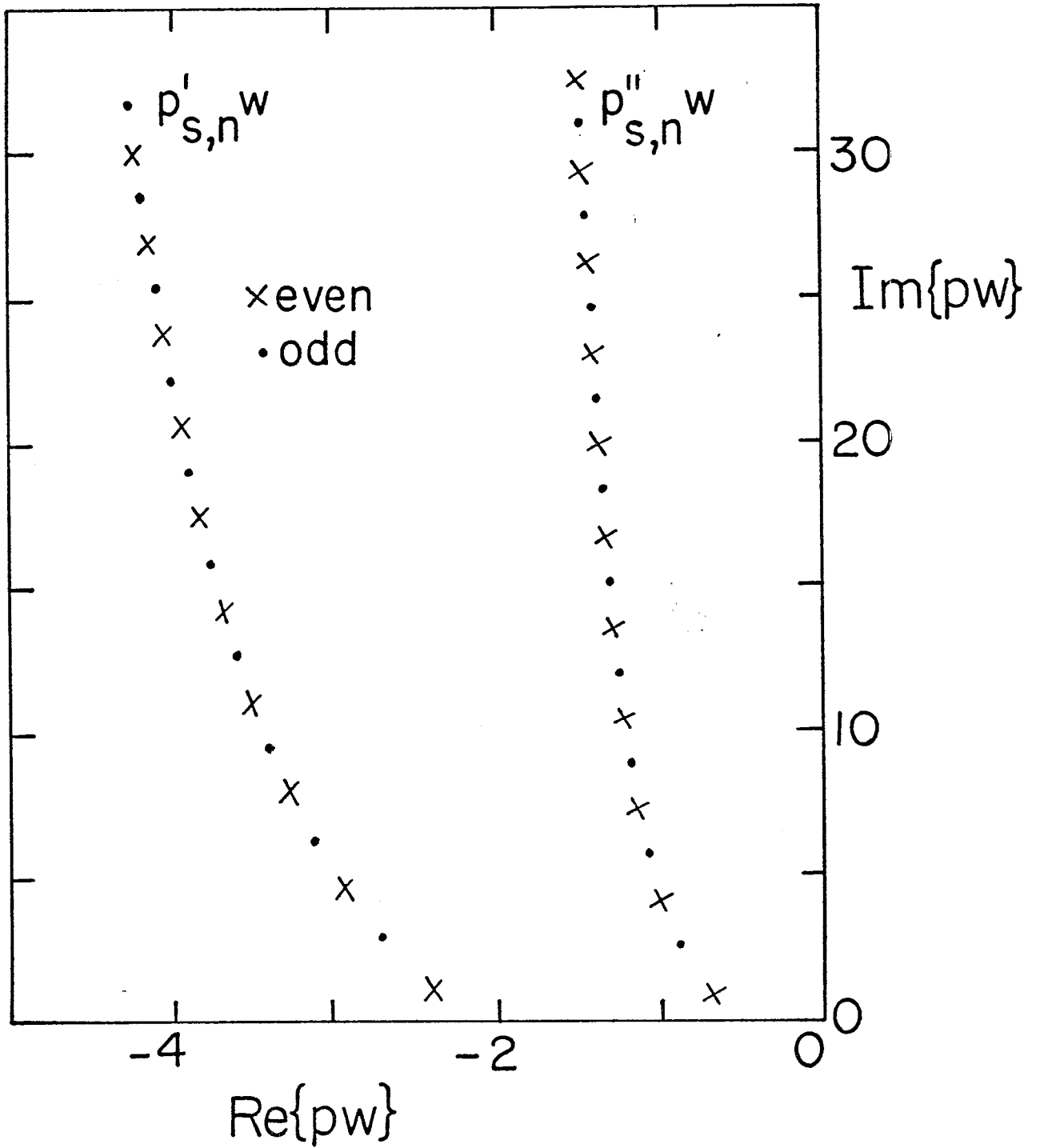


Figure 5. The transverse propagation constants for the symmetric TE modes ( $p''_{s,n}$ ) and the symmetric TM modes ( $p'_{s,n}$ ) in the limit as  $h/w$  tends to zero.

Table 1

Transverse complex propagation constants for the symmetric TE and TM modes as  $h/w \rightarrow 0$

Symmetric TE Modes				
even			odd	
n	$\text{Re}\{p_{s,n}^e\}$	$\text{Im}\{p_{s,n}^e\}$	$\text{Re}\{p_{s,n}^o\}$	$\text{Im}\{p_{s,n}^o\}$
1	-0.6863	1.0313	-0.8913	2.6683
2	-1.0019	4.2620	-1.0783	5.8449
3	-1.1368	7.4233	-1.1842	8.9994
4	-1.2240	10.5741	-1.2584	12.1479
5	-1.2886	13.7211	-1.3155	15.2938
Symmetric TM Modes				
even			odd	
n	$\text{Re}\{p_{s,n}^e\}$	$\text{Im}\{p_{s,n}^e\}$	$\text{Re}\{p_{s,n}^o\}$	$\text{Im}\{p_{s,n}^o\}$
1	-2.4024	1.1100	-2.7184	2.9796
2	-2.9562	4.6828	-3.1390	6.3306
3	-3.2868	7.9528	-3.4106	9.5605
4	-3.5172	11.1593	-3.6107	12.7521
5	-3.6939	14.3408	-3.7689	15.9264

SECTION III  
LONGITUDINAL COMPLEX WAVE NUMBERS

The variation of each mode can be separated into its transverse and longitudinal variation in the following manner

$$F_n(x, y, z) = F_n(x, y) \exp(\zeta_n z) \quad (5)$$

where  $F_n(x, y, z)$  denotes an arbitrary field component and  $\zeta_n$  is the longitudinal complex wavenumber given by

$$\zeta_n \equiv -\alpha_n + i\beta_n = i\sqrt{k^2 + p_n^2} \quad (6)$$

where  $k$  ( $= is/c$ ) is the free-space wave number. For a wave propagating in the positive  $z$  direction and with the harmonic time dependence  $\exp(-i\omega t)$  then both the damping constant  $\alpha_n$  and the propagation constant  $\beta_n$  in (6) are positive. For the square root on the right hand side of (6) to have a negative real part and a positive imaginary part requires that we choose  $p_n$  to be a root of (1) - (4) in the third quadrant.

From (6) it is clear that the imaginary part of  $p_n$  plays the role of cut off wave number in ordinary waveguide theory. However, due to the real part of  $p_n$ ,  $\zeta_n$  has always a negative real part. In fact, we have

$$\begin{aligned} \zeta_n &= \sqrt{k^2 + p_n^2} = \sqrt{k^2 + p_{nr}^2 - p_{ni}^2 + 2ip_{nr}p_{ni}} \\ &\approx \sqrt{k^2 - p_{ni}^2} + 2ip_{nr}p_{ni} / \sqrt{k^2 - p_{ni}^2} \end{aligned} \quad (7)$$

when  $k^2 > p_{ni}^2$  and since  $|p_{nr}| \ll |p_{ni}|$ . Here,  $p_{nr}$  ( $p_{ni}$ ) is the real (imaginary) part of  $p_n$ . From (7) and the results of the previous section that  $|p_{nr}|$  is much larger for antisymmetric TE modes than it is for symmetric TE and TM modes we draw the conclusion that the damping constants  $\alpha_n$  for the

antisymmetric TE modes are larger than those for the symmetric TE and TM modes. Thus, the most important higher-order modes on two wide parallel plates are the antisymmetric TE modes.

The propagation constants and the damping constants are plotted versus frequency in figures 6 and 7 for the four fundamental even and odd antisymmetric TE modes when  $h/w = 0.01$ . From these plots we observe that the fundamental odd antisymmetric TE mode has the lowest "cut-off" frequency.

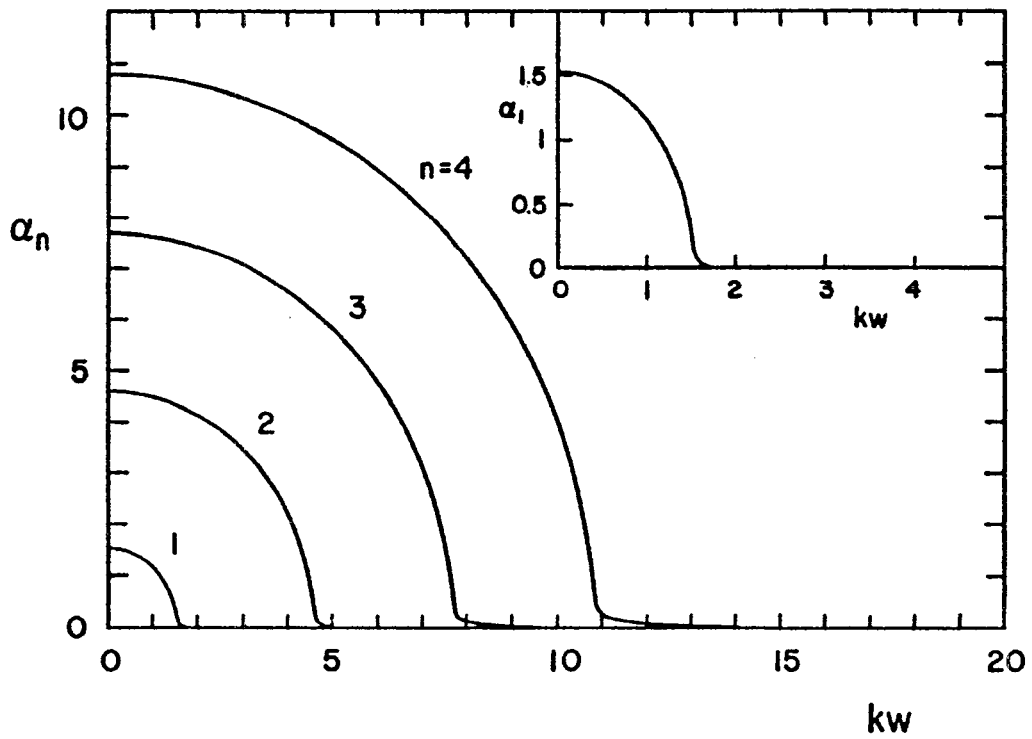
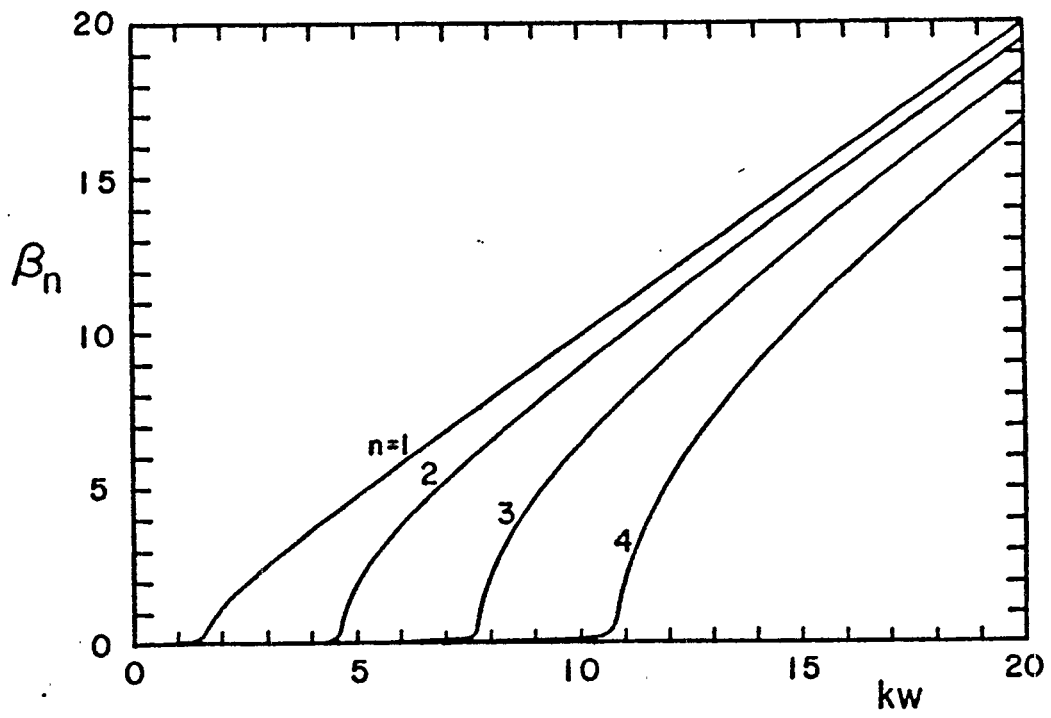


Figure 6. Frequency variation of propagation constant ( $\beta_n$ ) and attenuation constant ( $\alpha_n$ ) of the odd, antisymmetric, higher-order TE modes when  $h/w = 0.01$ .

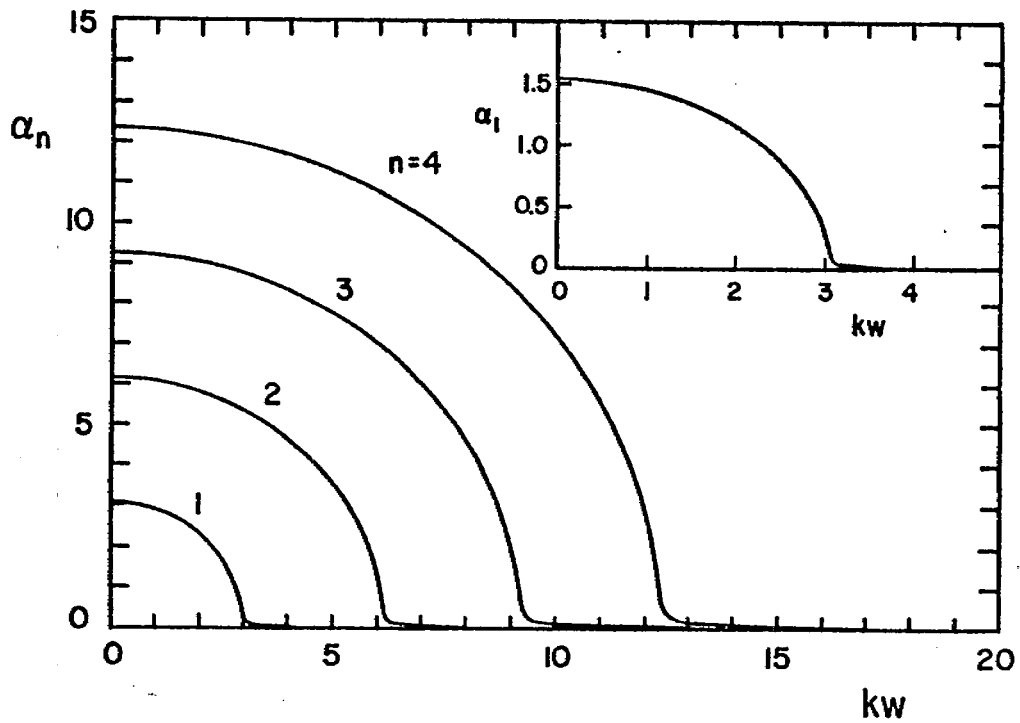
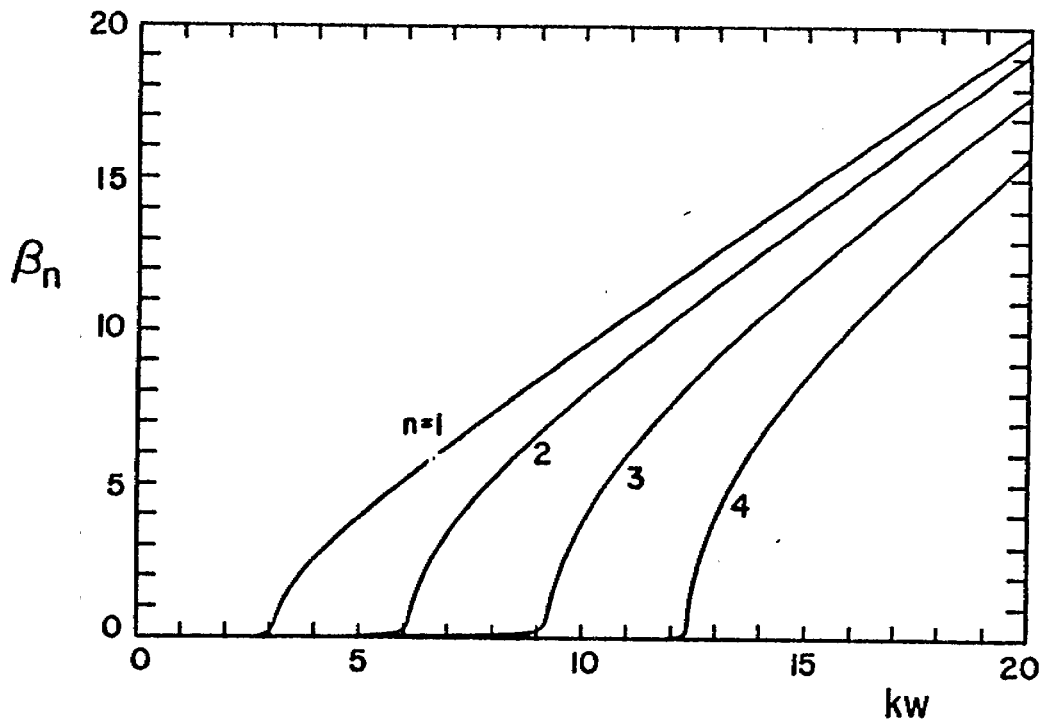


Figure 7. Frequency variation of propagation constant ( $\beta_n$ ) and attenuation constant ( $\alpha_n$ ) of the even, antisymmetric, higher-order TE modes when  $h/w = 0.01$ .

SECTION IV  
MODAL FIELD DISTRIBUTION

Analytical expressions for the field components of the antisymmetric TE modes which are valid in the region between the two parallel plates are derived in ref. 8. It is found in that reference that the field components of the even, antisymmetric TE modes are given by

$$\begin{aligned} \underline{H}_n^e &= H_0 \left[ \left( \zeta_n^e / p_{n,a}''^e \right) \cosh(p_{n,a}''^e x) \hat{x} + \sinh(p_{n,a}''^e x) \hat{z} \right] \exp(\zeta_n^e z) \\ \underline{E}_n^e &= i H_0 Z_0 (k / p_{n,a}''^e) \cosh(p_{n,a}''^e x) \exp(\zeta_n^e z) \hat{y} \end{aligned} \quad (8)$$

where

$$\zeta_n^e = i \sqrt{k^2 + (p_{n,a}''^e)^2}$$

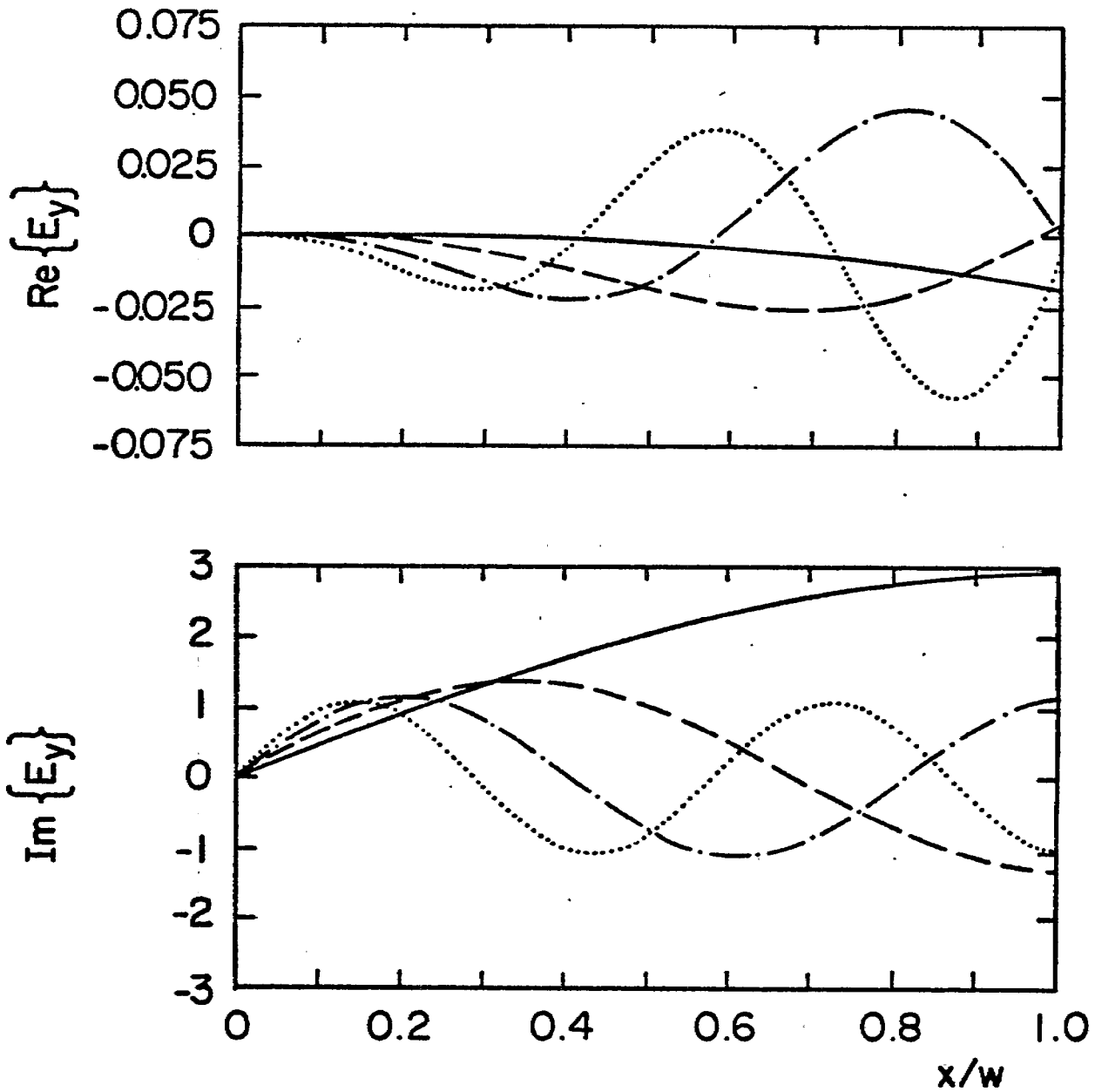
and  $H_0$  is an arbitrary constant.

Similarly, it was found in ref. 8 that the field components of the odd, antisymmetric TE modes are given by

$$\begin{aligned} \underline{H}_n^o &= H_0 \left[ \left( \zeta_n^o / p_{n,a}''^o \right) \sinh(p_{n,a}''^o x) \hat{x} + \cosh(p_{n,a}''^o x) \hat{z} \right] \exp(\zeta_n^o z) \\ \underline{E}_n^o &= i H_0 Z_0 (k / p_{n,a}''^o) \sinh(p_{n,a}''^o x) \exp(\zeta_n^o z) \hat{y} \end{aligned} \quad (9)$$

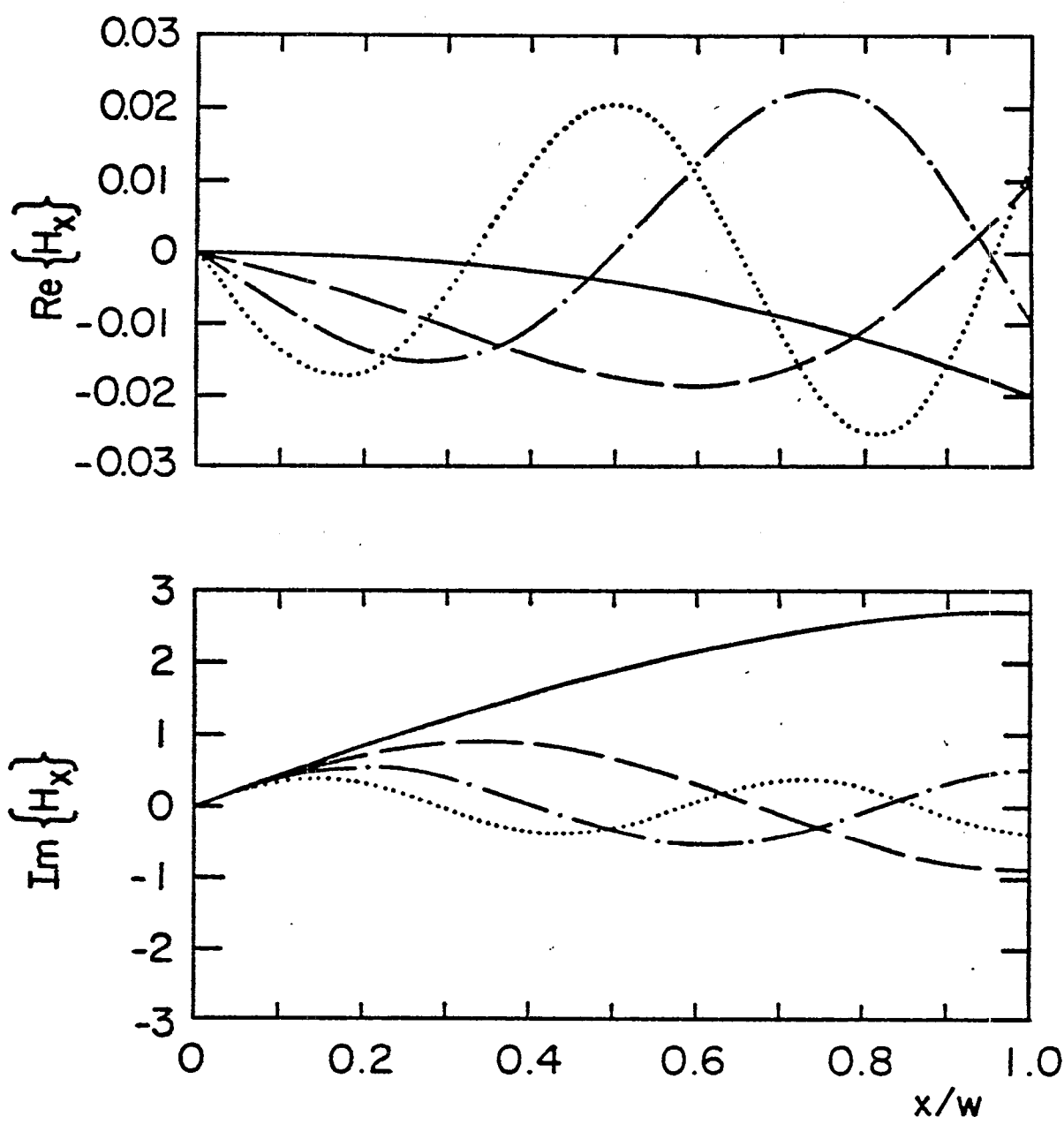
1. *Transverse Field Distribution*

The transverse field distributions of the four fundamental even and odd antisymmetric TE modes are presented in figures 8a through 9c (when  $h/w = 0.01$ ). These curves were obtained by putting  $H_0 = 0$  and  $z = 0$  in (8) and (9). To obtain the curves for the  $x$  component of the magnetic field and the  $y$  component of the electric field requires that we choose a particular value of the free-space wave number  $k$ . This wave number ( $k_n$ ) is chosen so that the guided wavelength  $\lambda_g$  of each mode is  $1.5 w$ ; i.e.,  $k_n$  is determined from the following equation



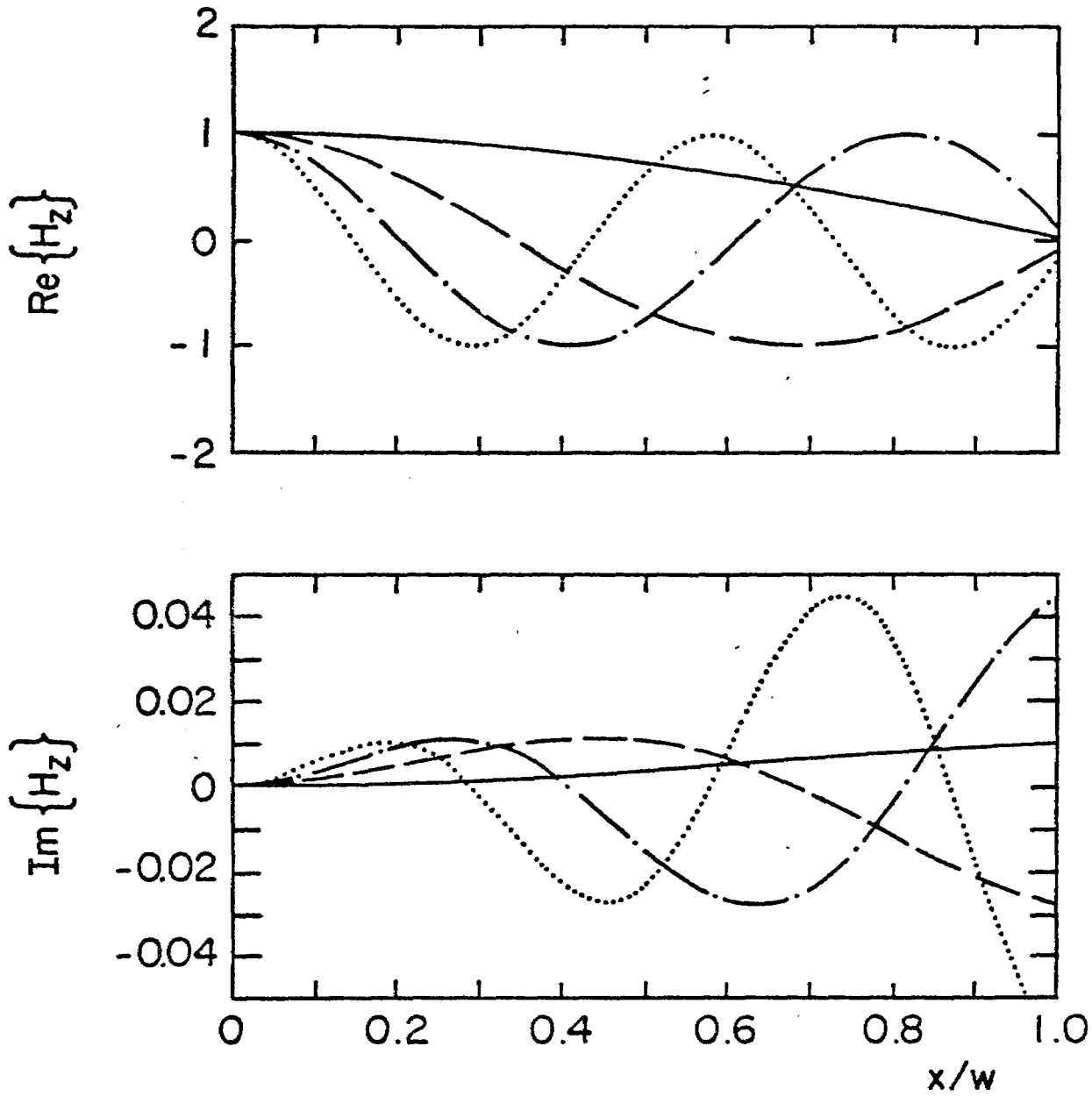
$\rho w = -0.010 - i1.54$  ———,  $-0.028 - i4.62$  ———,   
 $-0.045 - i7.71$  - · - · - ·,  $-0.062 - i10.81$  ······ .

Figure 8a. Transverse variation of the  $E_y$  field component of the four lowest odd antisymmetric TE modes.



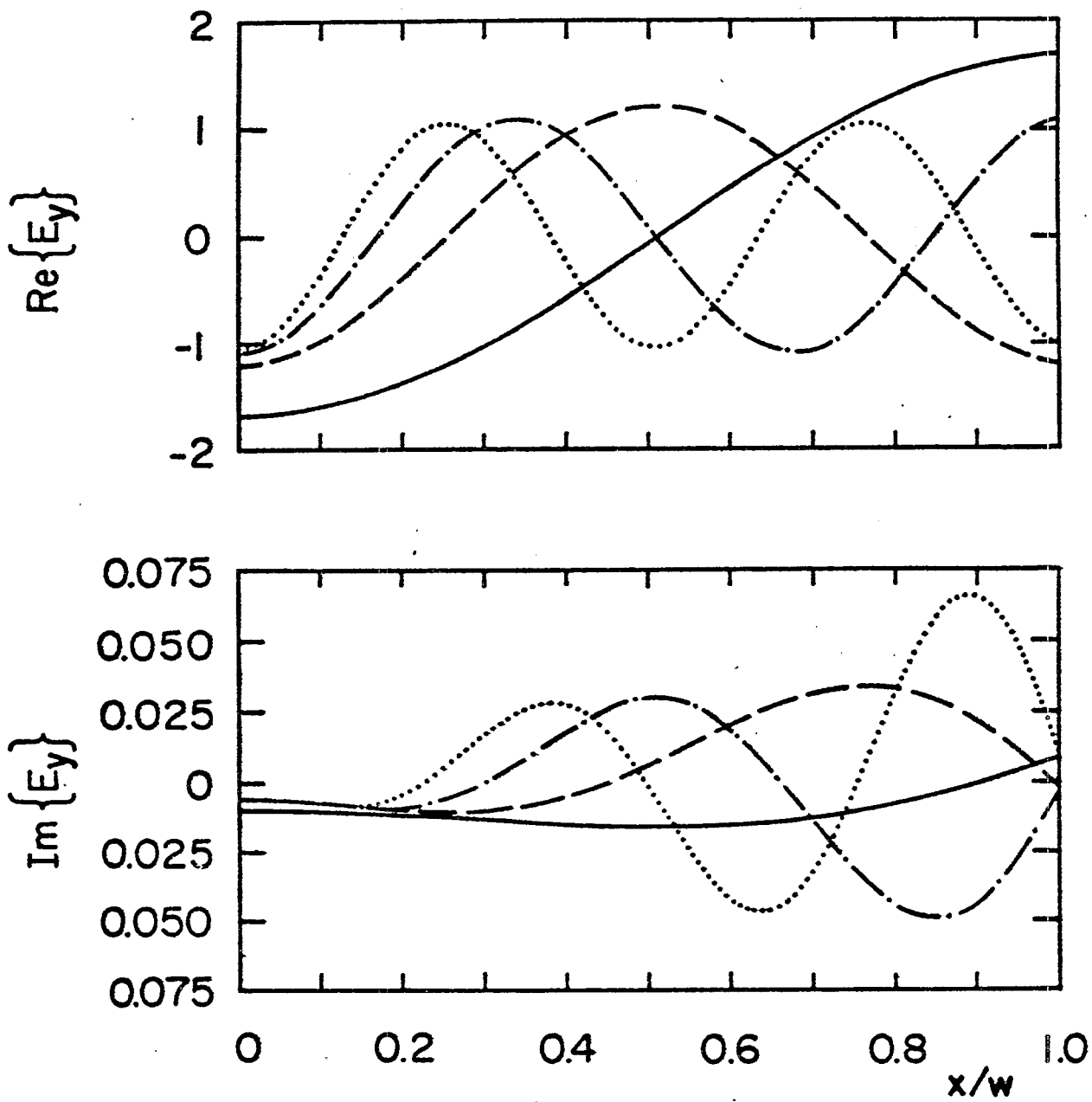
$pw = -0.010 - i1.54$  ———,  $-0.028 - i4.62$  ----,   
 $-0.045 - i7.71$  -·-·-·-,  $-0.062 - i10.81$  .....

Figure 8b. Transverse variation of the  $H_x$  field component of the four lowest odd antisymmetric TE modes.



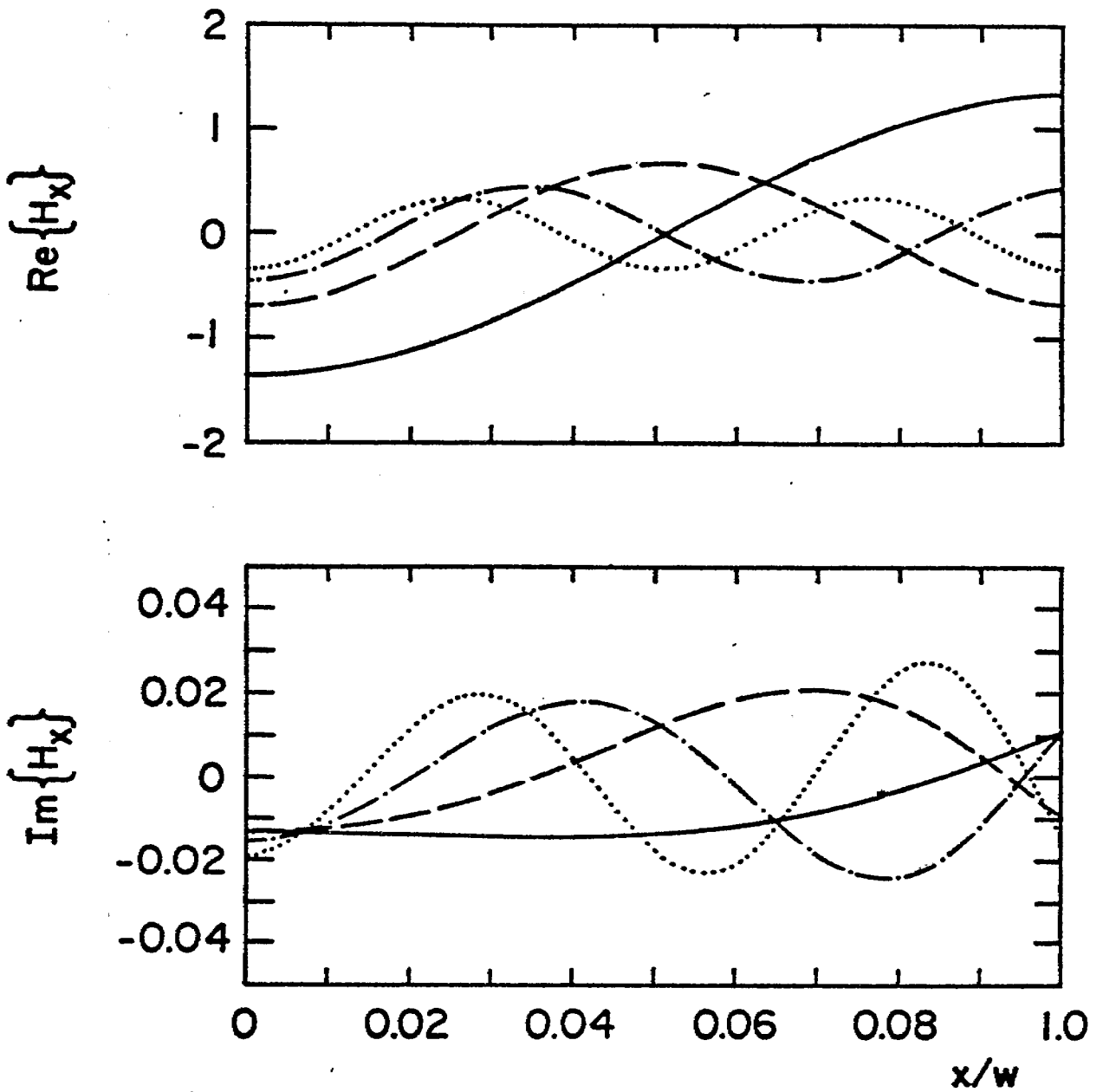
$\rho w = -0.010 - i1.54$  ———,  $-0.028 - i4.62$  ----,   
 $-0.045 - i7.71$  - · - · - ·,  $-0.062 - i10.81$  .....

Figure 8c. Transverse variation of the  $H_z$  field component of the four lowest odd antisymmetric TE modes.



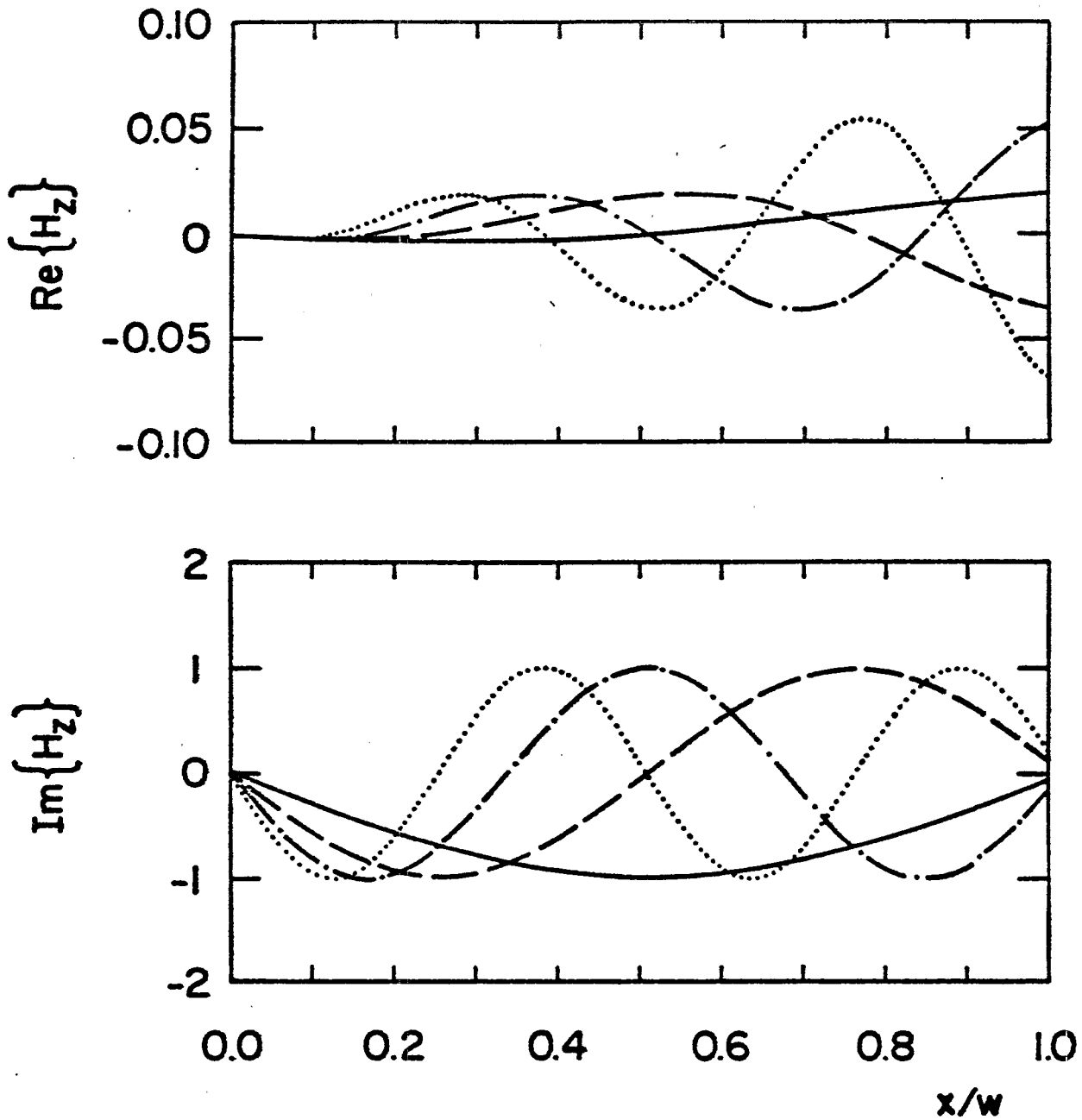
$\rho w = -0.019 - i3.08$  ———,  $-0.036 - i6.16$  ----,   
 $-0.053 - i9.26$  -·-·-·-,  $-0.070 - i12.35$  ······.

Figure 9a. Transverse variation of the  $E_y$  field component of the four lowest even antisymmetric TE modes.



$p_w = -0.019 - i3.08$  ———,  $-0.036 - i6.16$  — — —,   
 $-0.053 - i9.26$  - - - - -,  $-0.070 - i12.35$  .....

Figure 9b. Transverse variation of the  $H_x$  field component of the four lowest even antisymmetric TE modes.



$\rho w = -0.019 - i3.08$  ———,  $-0.036 - i6.16$  ———,   
 $-0.053 - i9.26$  -·-·-·-,  $-0.070 - i12.35$  ······.

Figure 9c. Transverse variation of the  $H_z$  field component of the four lowest even antisymmetric TE modes.

$$\beta_n = \text{Re} \left\{ \sqrt{k_n^2 + p_n^2} \right\} = 4\pi/3w . \quad (10)$$

The reason for this choice of  $k_n$  will become obvious in the next subsection.

## 2. Vector Representation

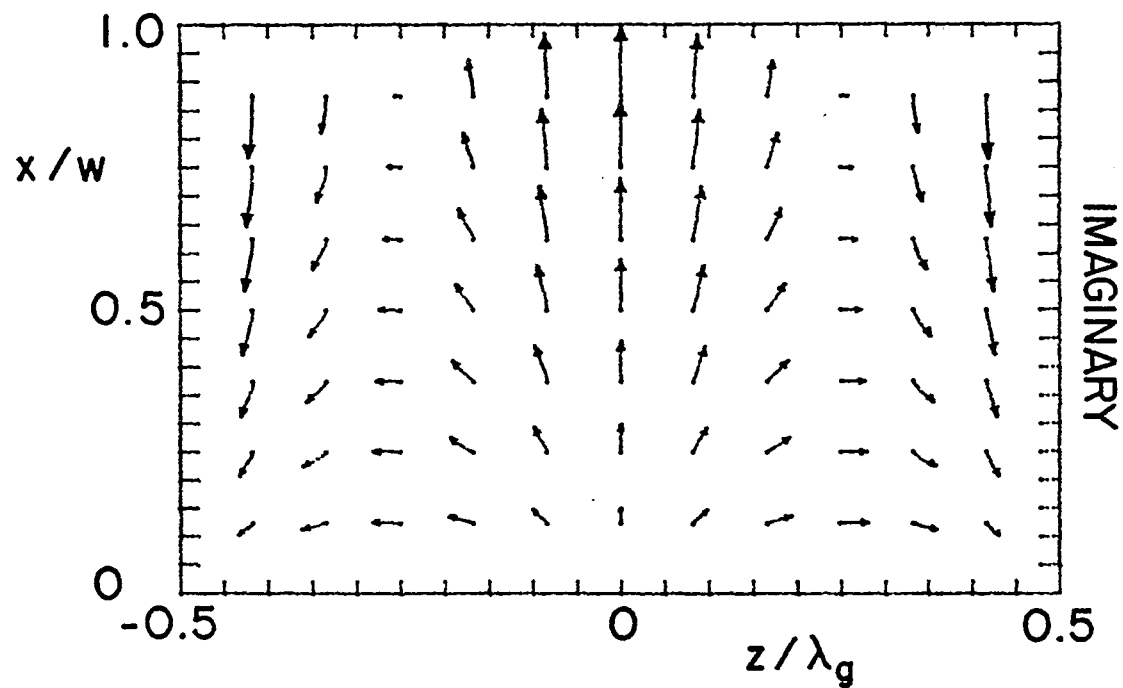
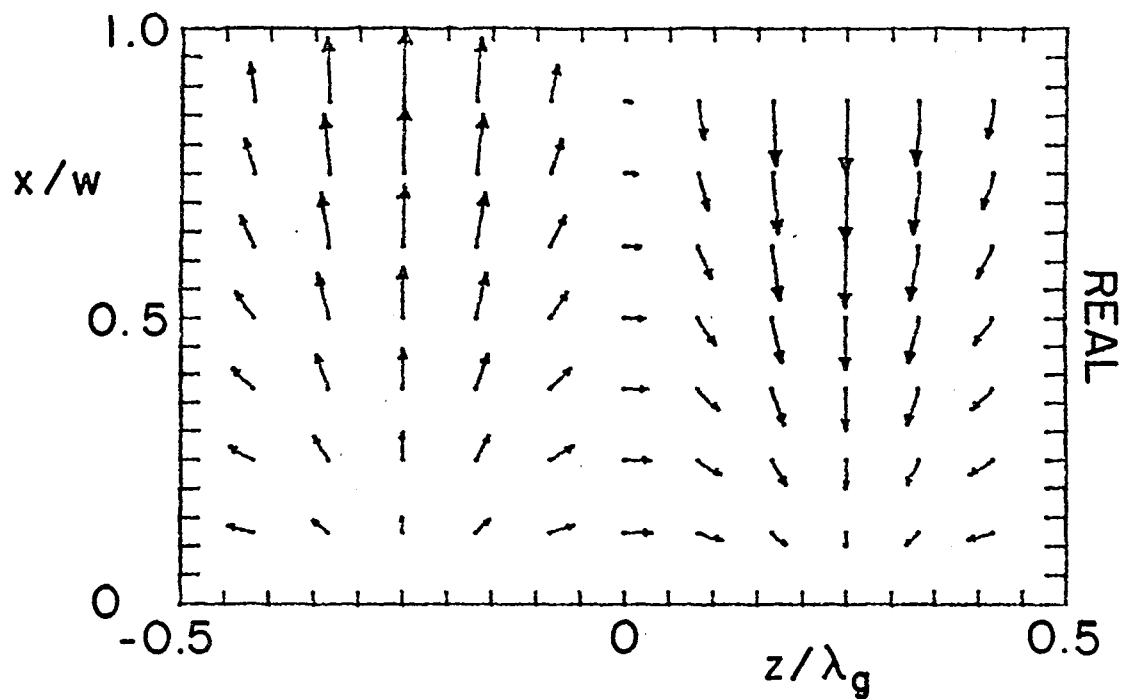
One way of depicting the H-field in the  $x, z$  plane is the use of a vector plot. In this plot the magnitude and direction of the real and imaginary parts of the magnetic field is visualized by arrows at certain regularly spaced lattice points (the base of the arrow). The size of the arrow is proportional to the field strength and the direction of the arrow shows the field direction. Figures 10a through 11d show vector plots for the four fundamental even and odd antisymmetric TE modes when  $h/w = 0.01$ .

Some comments are in order concerning figures 10a through 11d. First, both the real and imaginary parts of one particular mode have been normalized with the same constant. Therefore, the vector plots show the relative magnitude, direction, and phase for each mode. Second, the  $x$ -coordinate in the vector plots have been normalized with respect to the half width  $w$  of the two plates, and the  $z$ -coordinate has been normalized with respect to the guided wavelength  $\lambda_g = 2\pi/\beta_n$  of each mode. As mentioned previously, the frequency (or free-space wave number) is chosen so that  $\lambda_g = 1.5 w$  for each mode. The value of  $k$  used for each mode is indicated on the respective graph. Thus, the  $z$  variable varies between  $-\lambda_g/2$  and  $\lambda_g/2$  (as shown in figures 10a through 11d) or between  $-3w/4$  and  $3w/4$  (as indicated by the frame size in figures 10a through 11d).

## 3. Field Lines

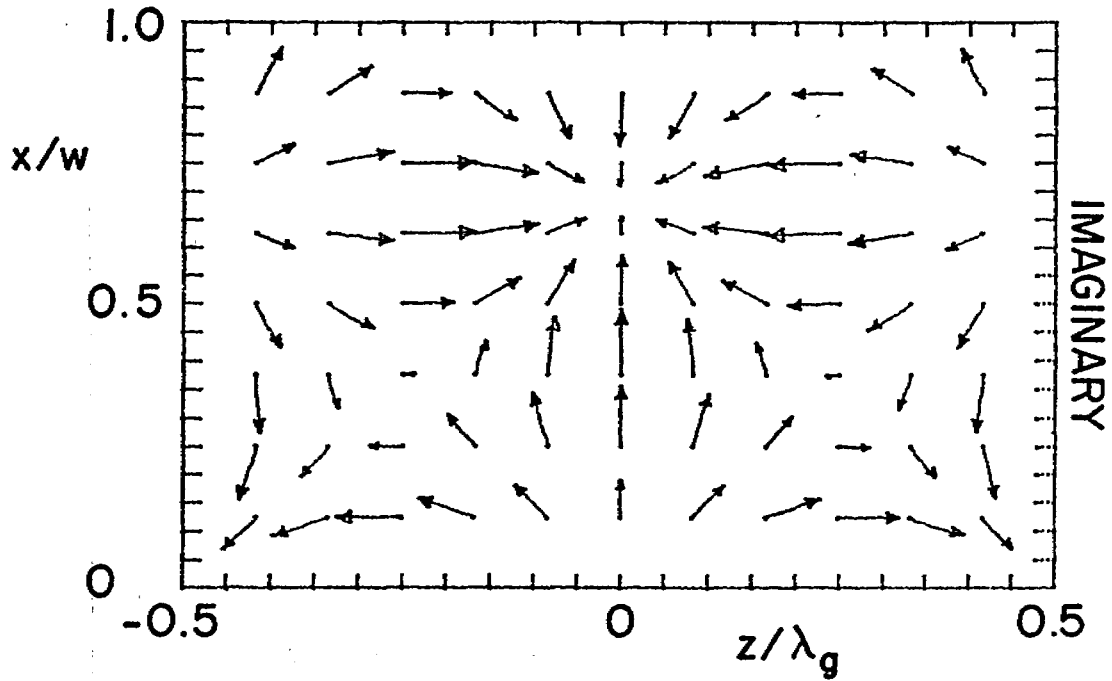
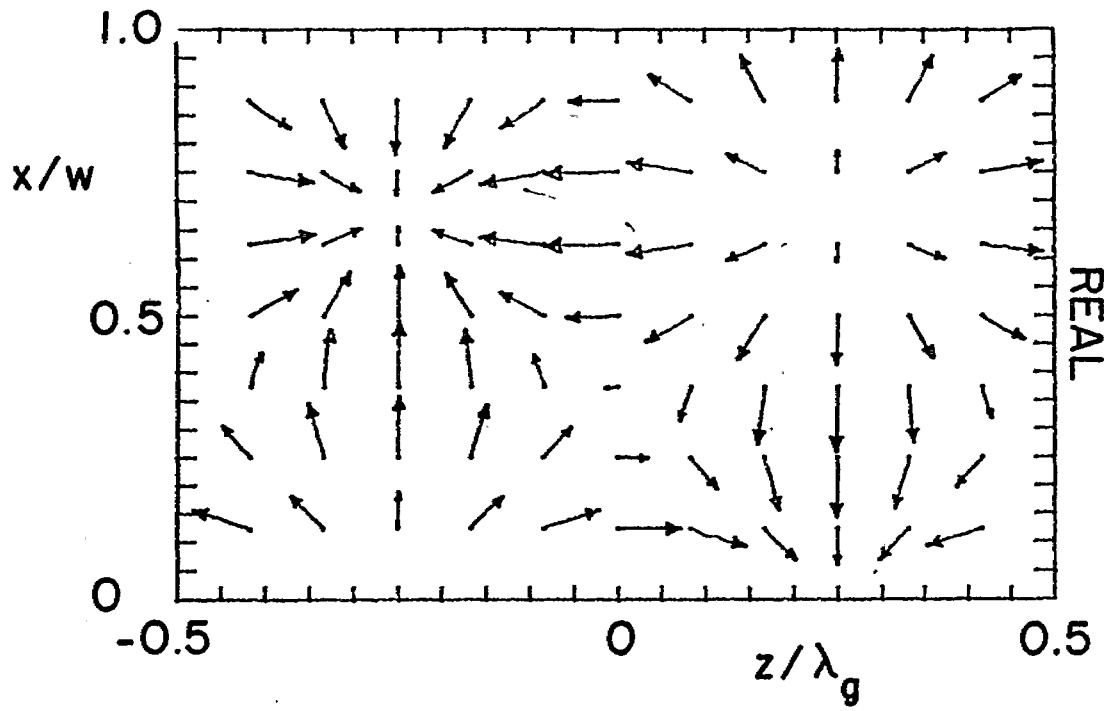
Another way of representing the magnetic field is the use of field lines. The magnetic field lines of the four lowest order even and odd antisymmetric TE modes are shown in figures 12a through 13d. We observe from these graphs that the magnetic field tangent to the  $x, z$  plane has apparent sources. These apparent sources can be understood from the following arguments:

1. According to (8) and (9) the magnetic field has no  $y$ -component. However, these expressions are approximate and the small  $y$ -component of the H-field has been omitted.



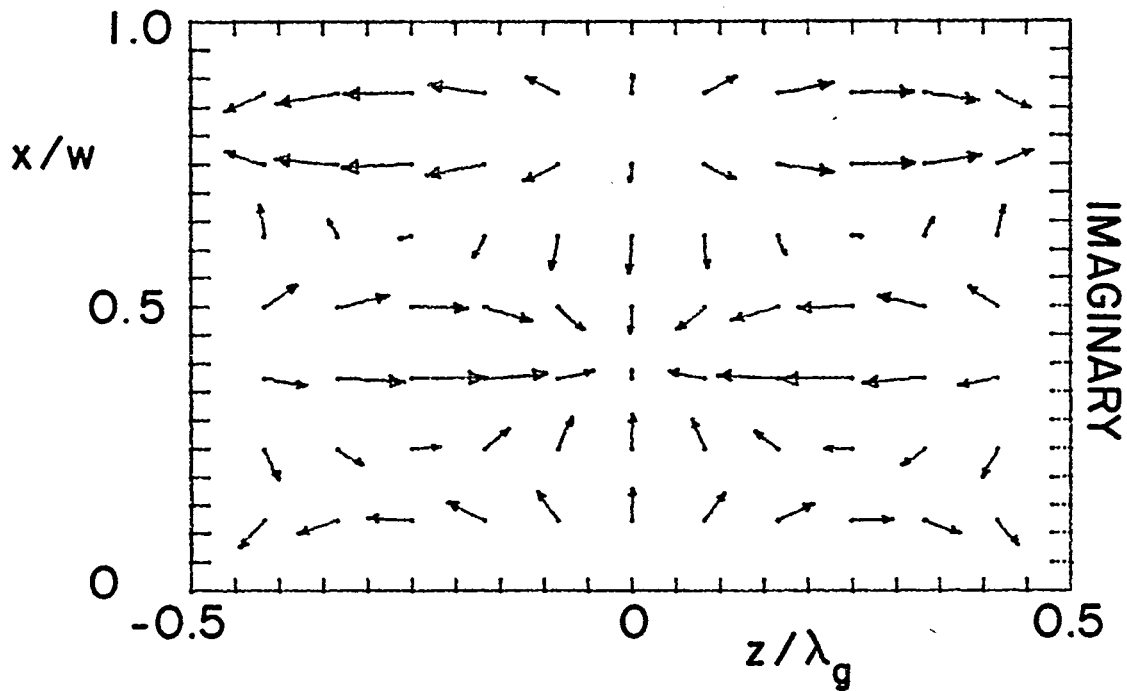
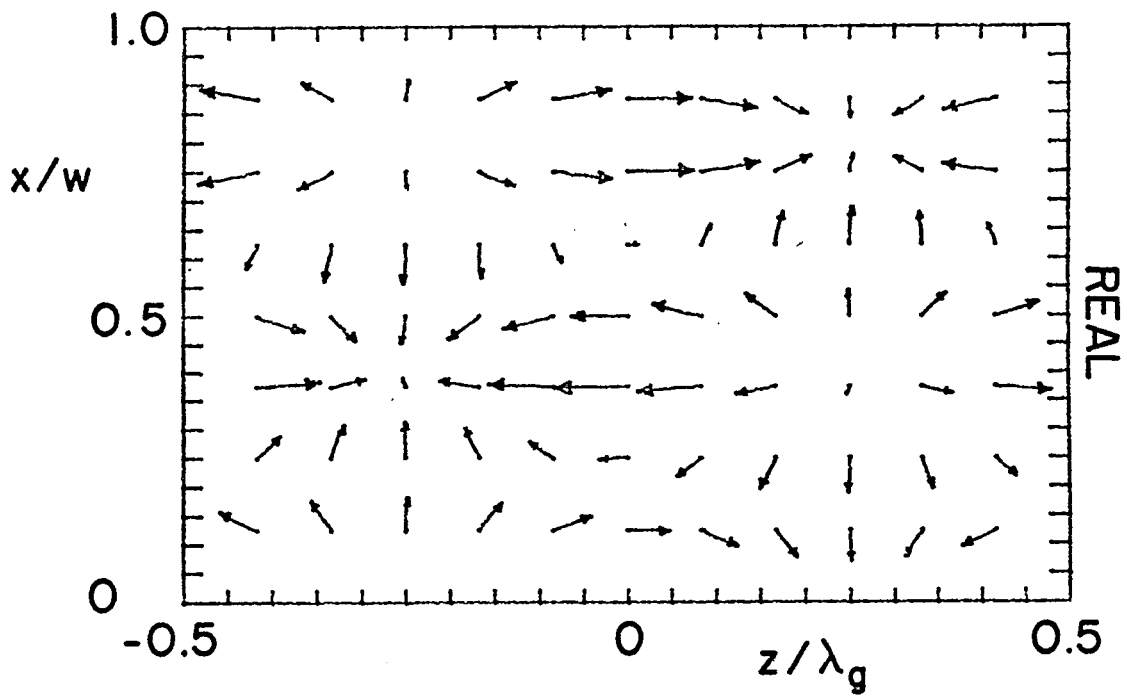
$$pw = -0.010 - i1.54, \quad kw = 4.46$$

Figure 10a. Vector diagram for the components tangential to the  $x, z$  plane of the magnetic field of the lowest odd antisymmetric TE mode.



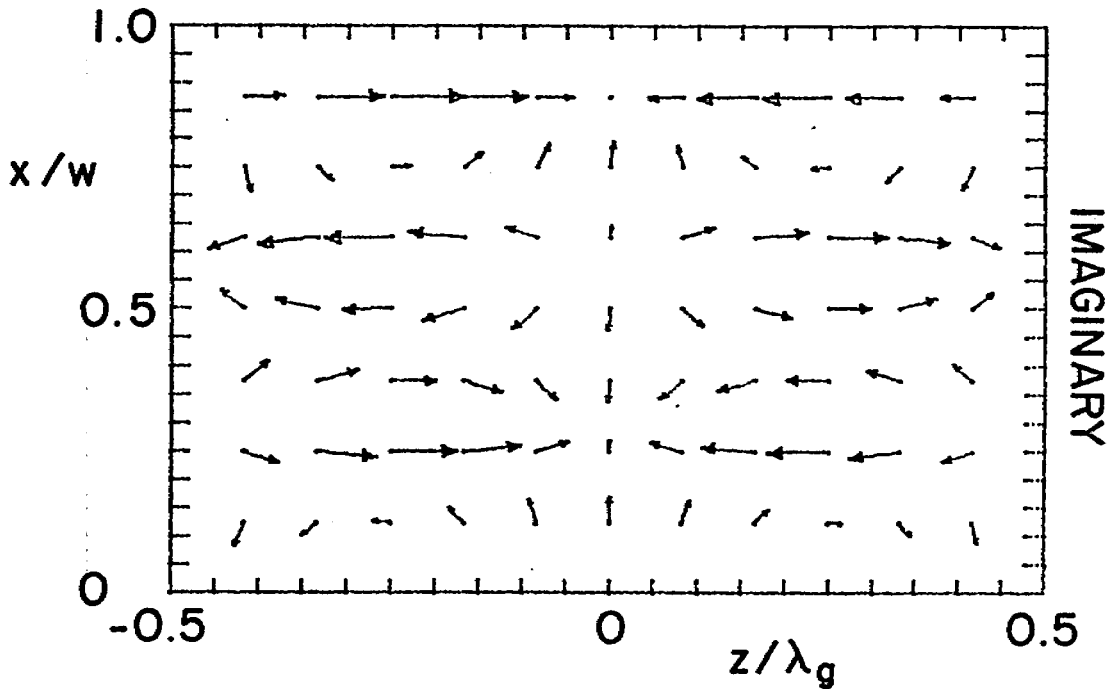
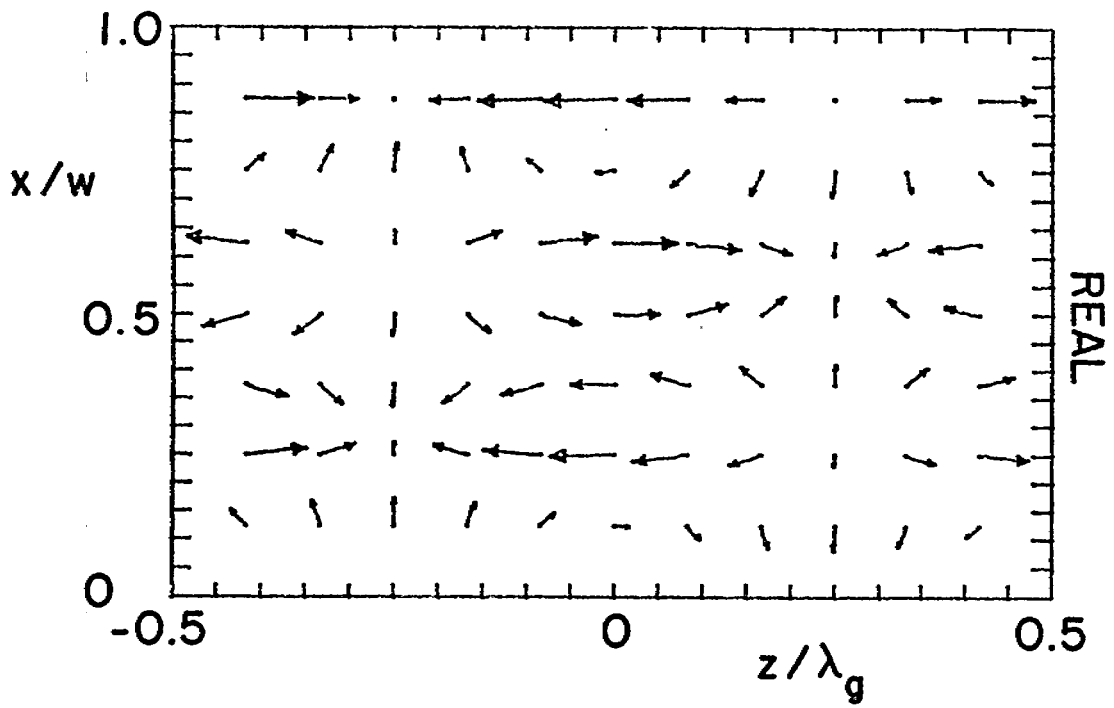
$$pw = -0.028 - i4.62, \quad kw = 6.24$$

Figure 10b. Vector diagram for the components tangential to the  $x,z$  plane of the magnetic field of the second lowest odd antisymmetric TE mode.



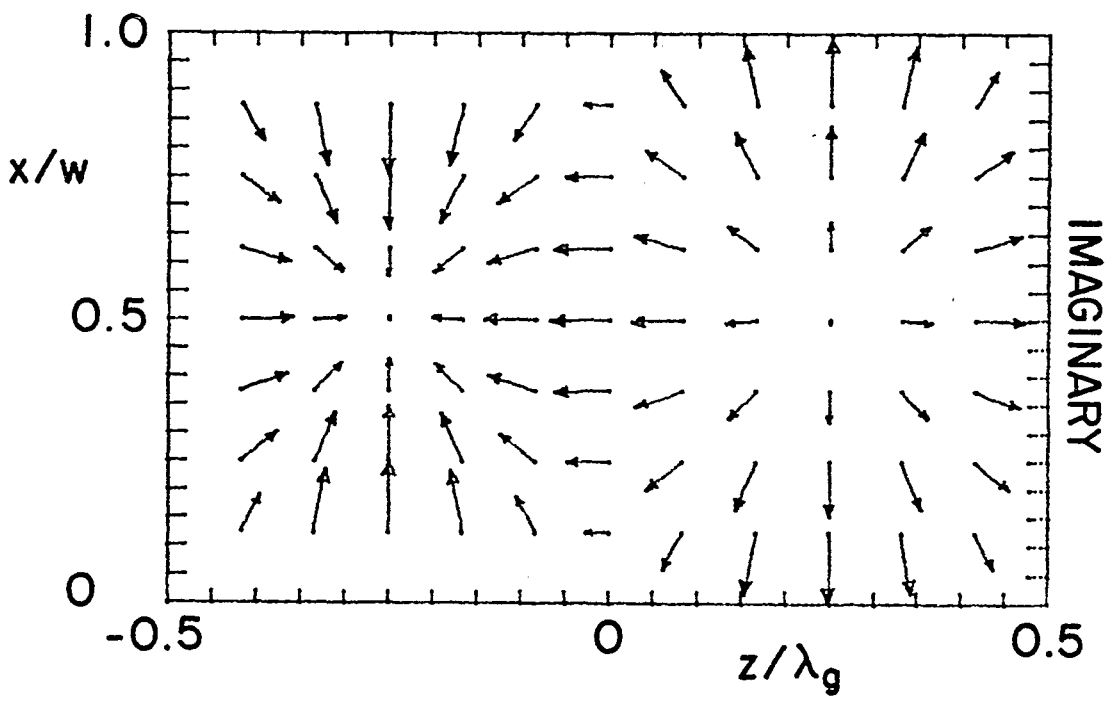
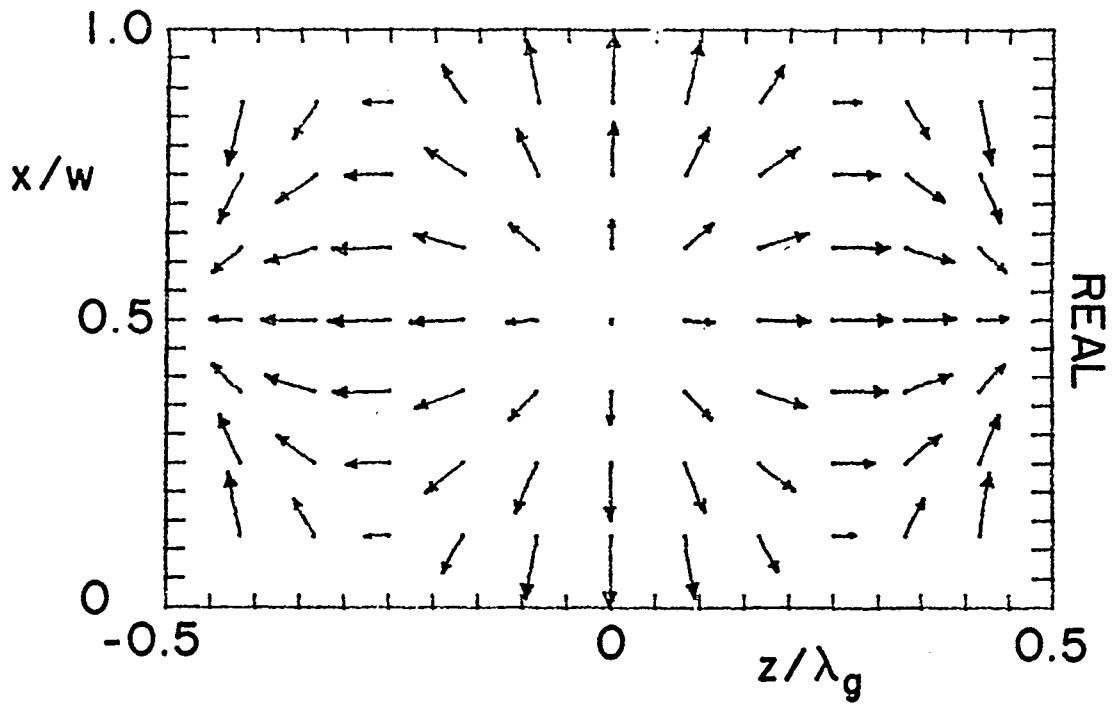
$$pw = -0.045 + i7.71, kw = 8.77$$

Figure 10c. Vector diagram for the components tangential to the  $x, z$  plane of the magnetic field of the third lowest odd antisymmetric TE mode.



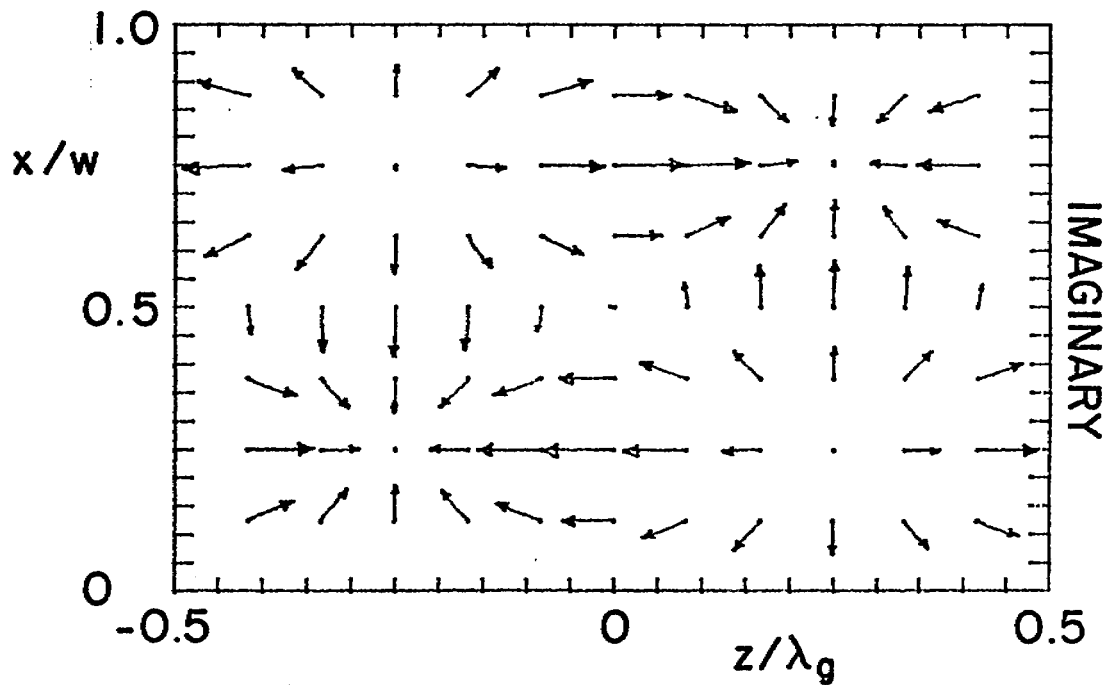
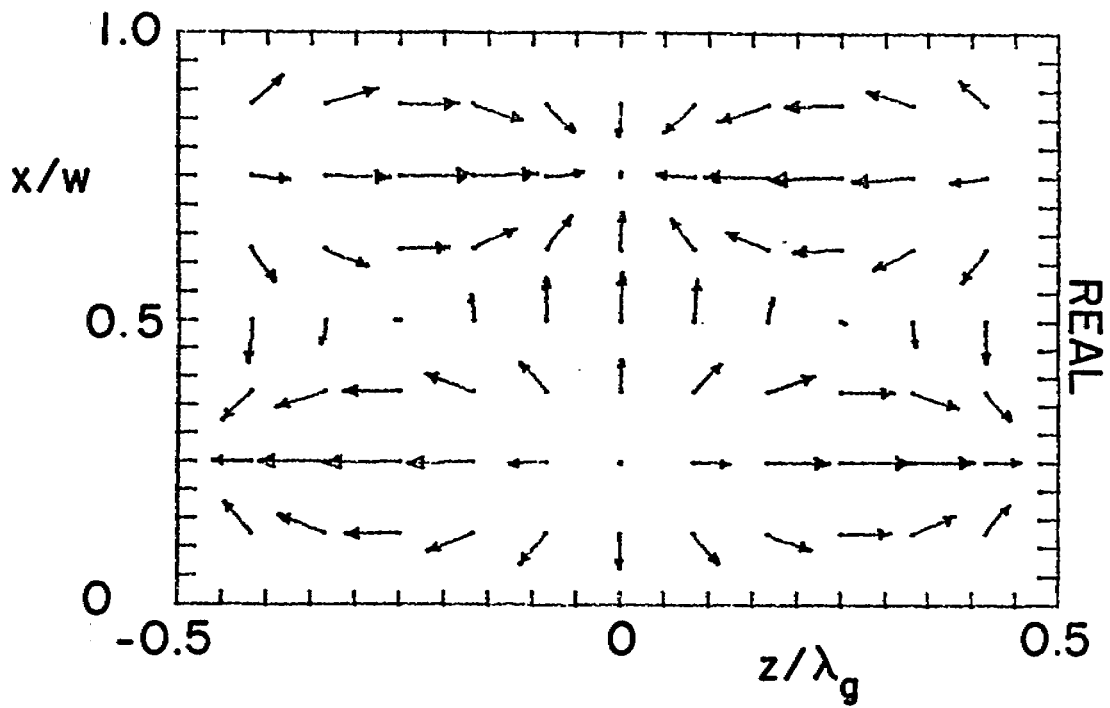
$$pw = -0.062 - i10.81, \quad kw = 11.59$$

Figure 10d. Vector diagram for the components tangential to the  $x, z$  plane of the magnetic field of the fourth lowest odd antisymmetric TE mode.



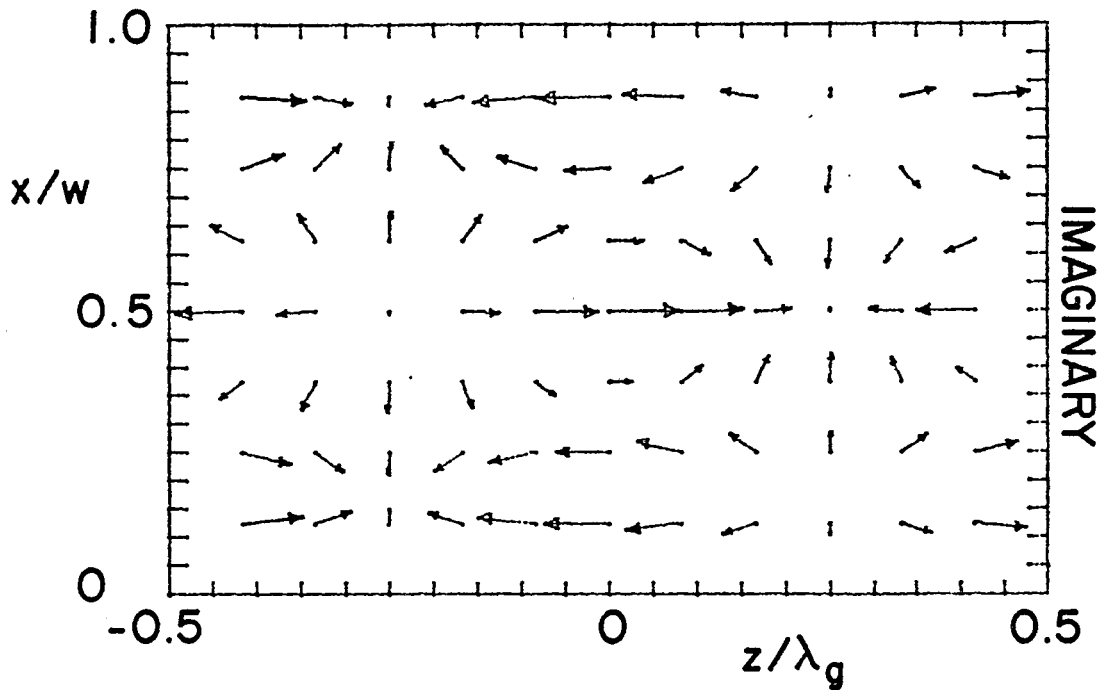
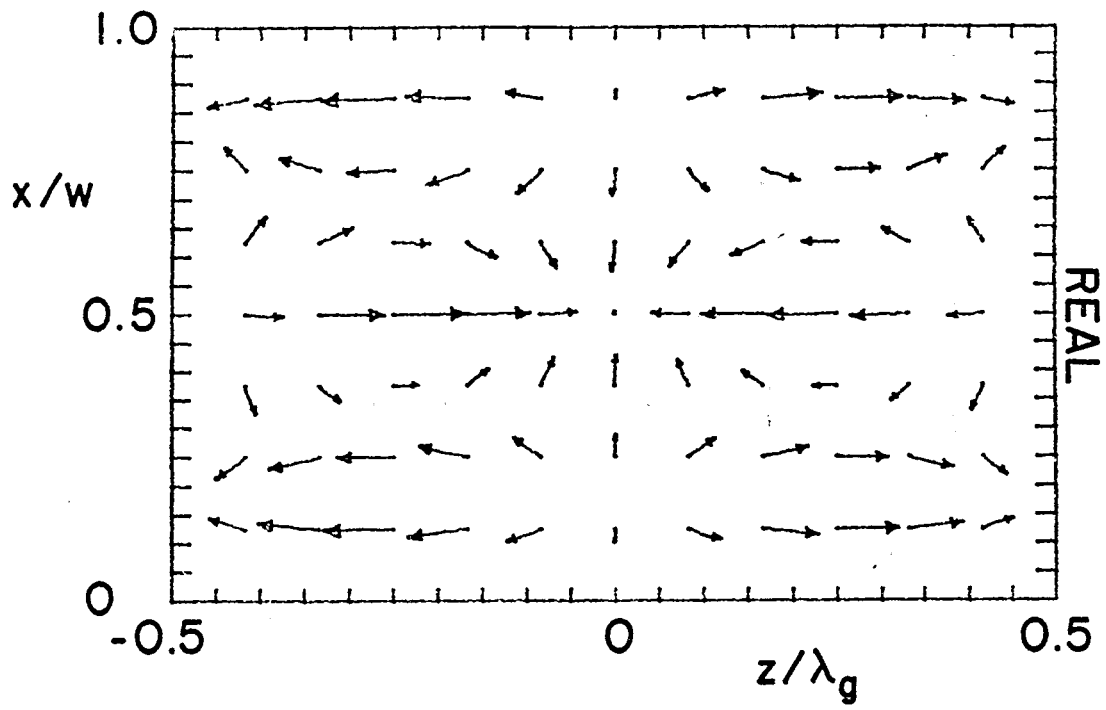
$$pw = -0.019 - i3.08, kw = 5.20$$

Figure 11a. Vector diagram for the components tangential to the  $x, z$  plane of the magnetic field of the lowest even antisymmetric TE mode.



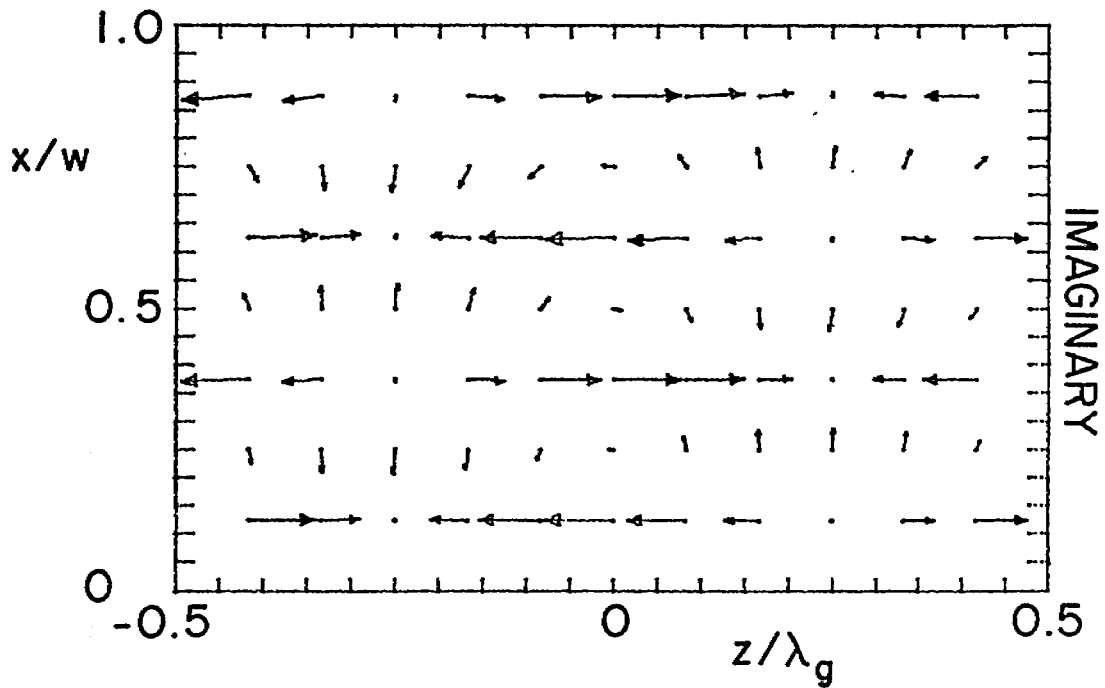
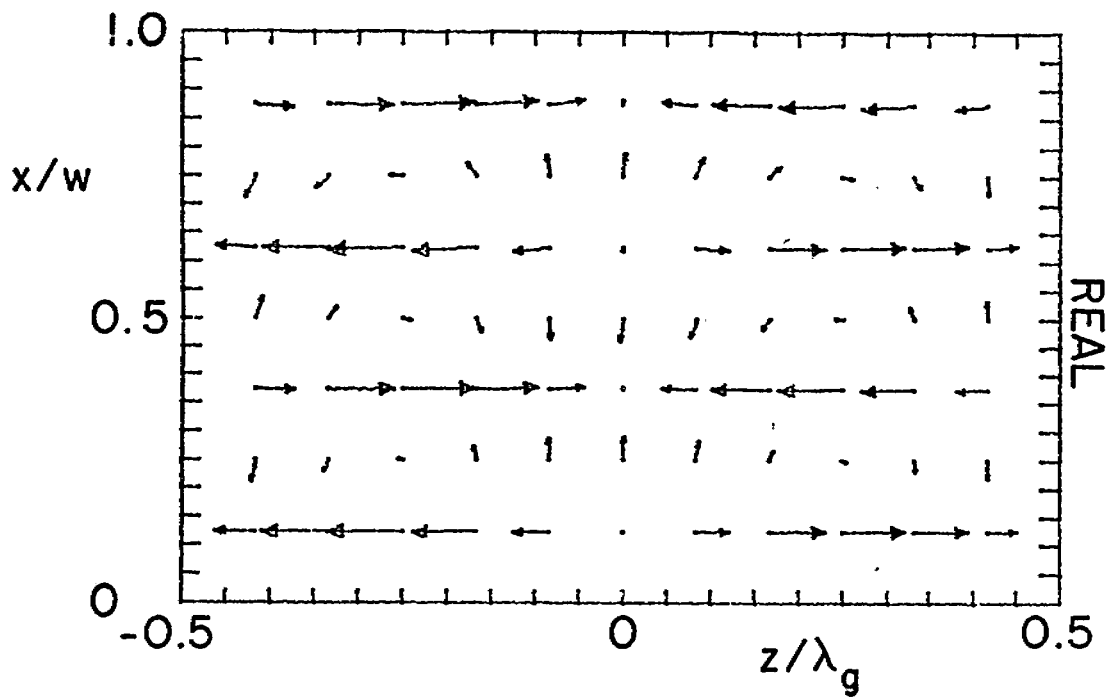
$$pw = -0.036 - i6.16, \quad kw = 7.45$$

Figure 11b. Vector diagram for the components tangential to the  $x, z$  plane of the magnetic field of the second lowest even antisymmetric TE mode.



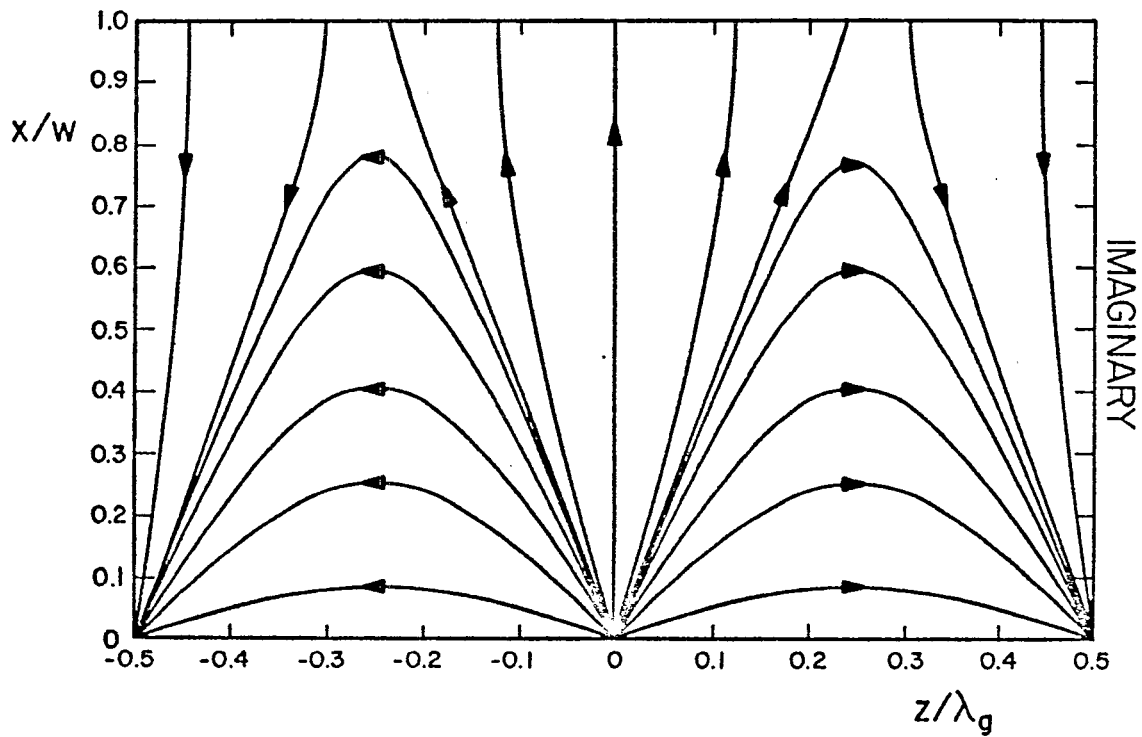
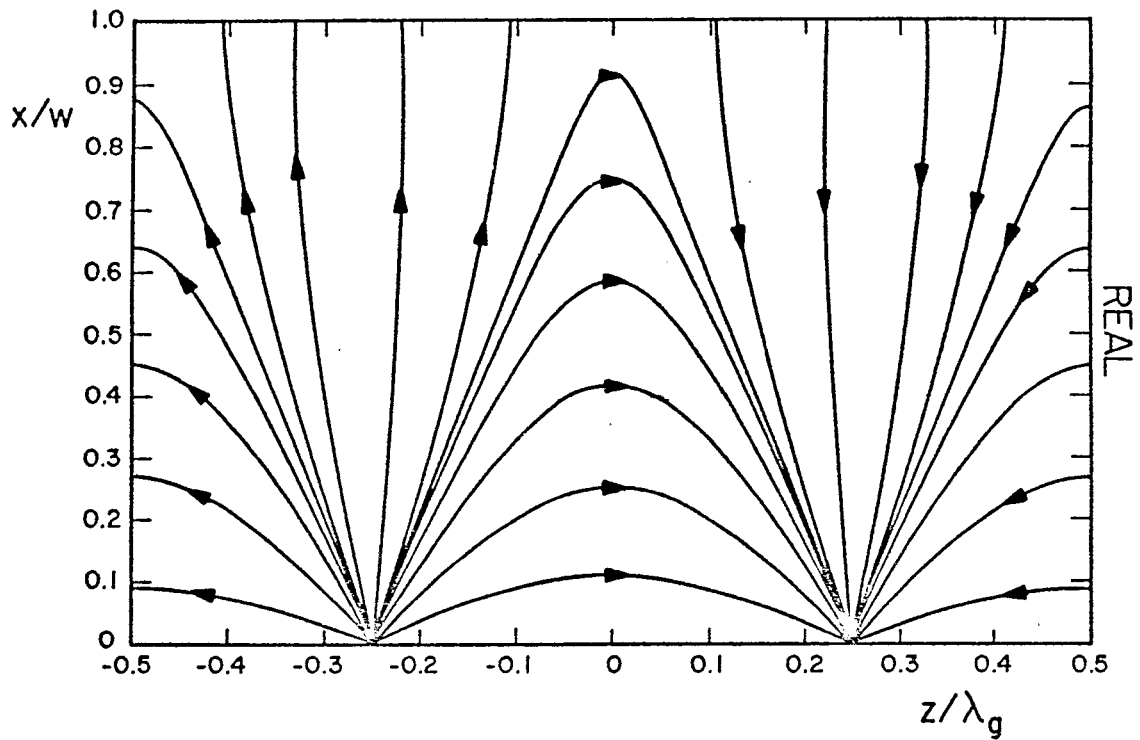
$$pw = -0.053 - i9.26, \quad kw = 10.16$$

Figure 11c. Vector diagram for the components tangential to the  $x, z$  plane of the magnetic field of the third lowest even anti-symmetric TE mode.



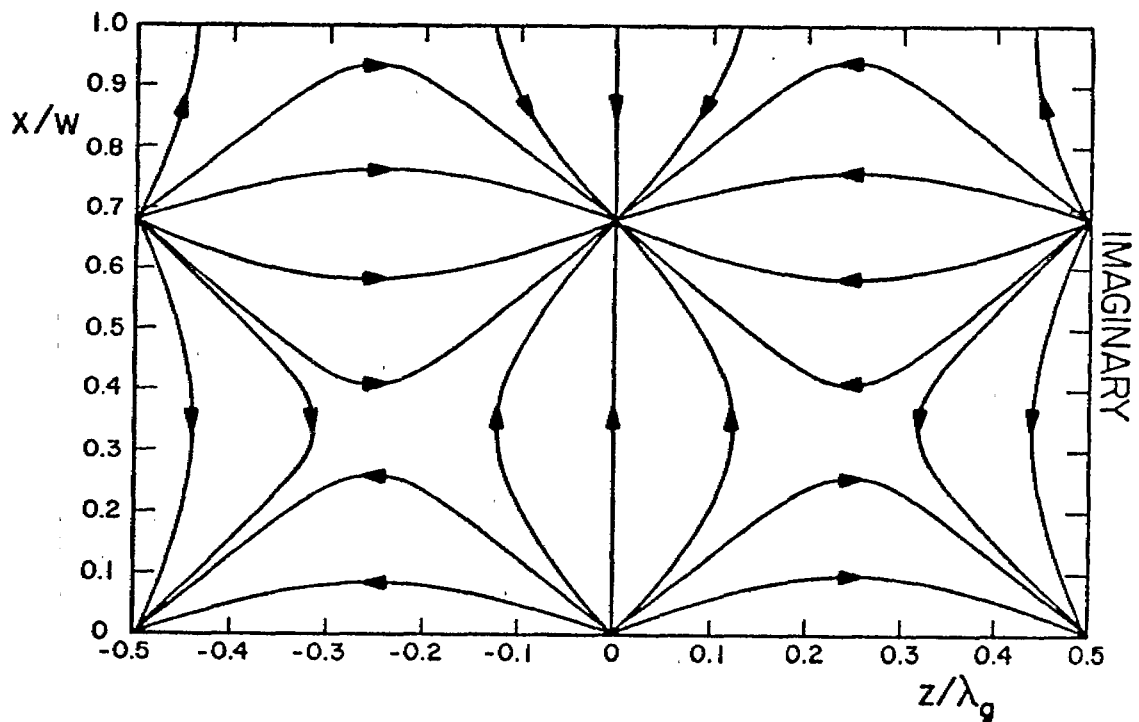
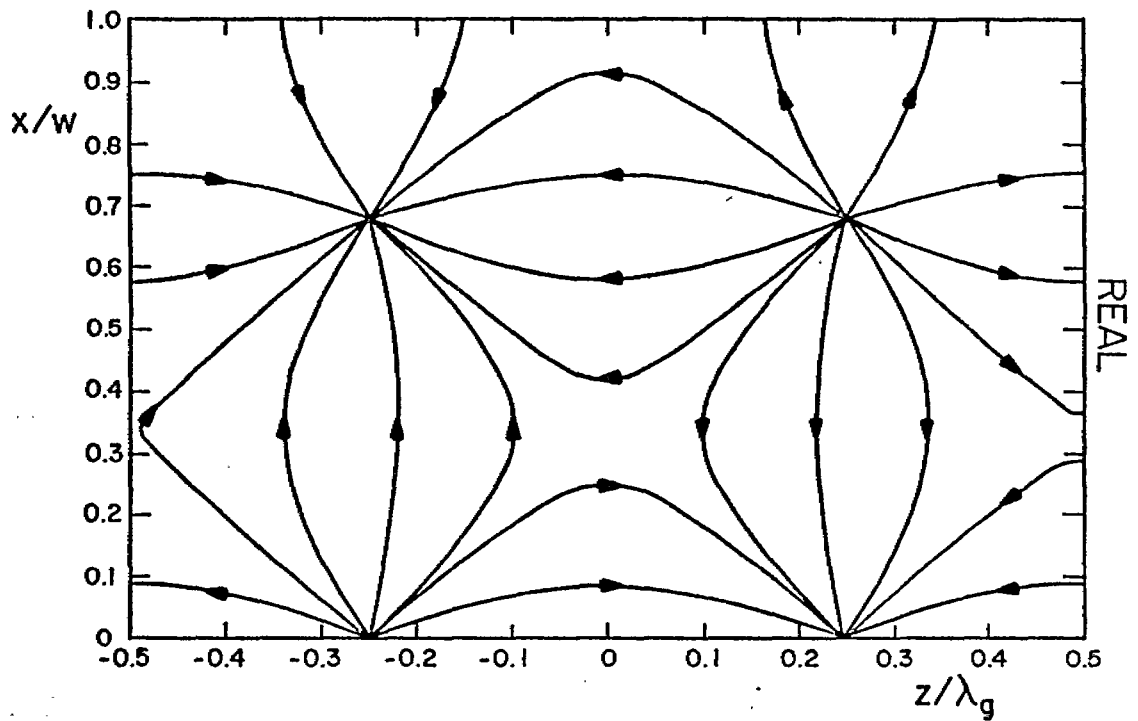
$$pw = -0.070 - i12.35, kw = 13.04$$

Figure 11d. Vector diagram for the components tangential to the  $x, z$  plane of the magnetic field of the fourth lowest even antisymmetric TE mode.



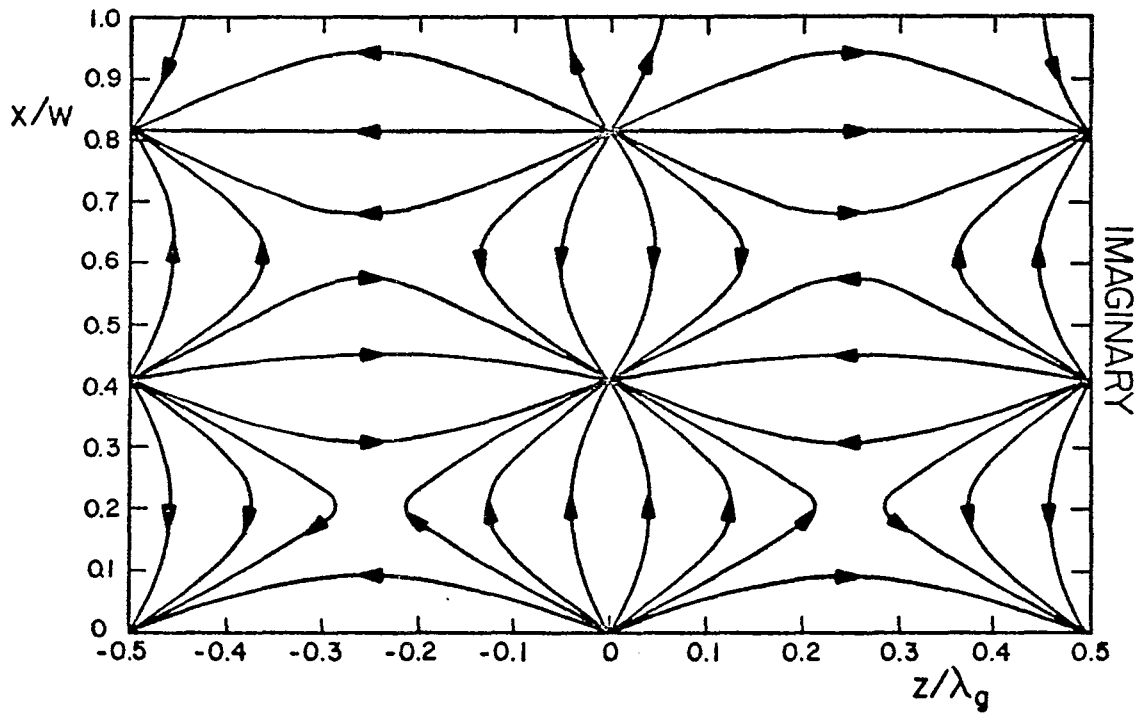
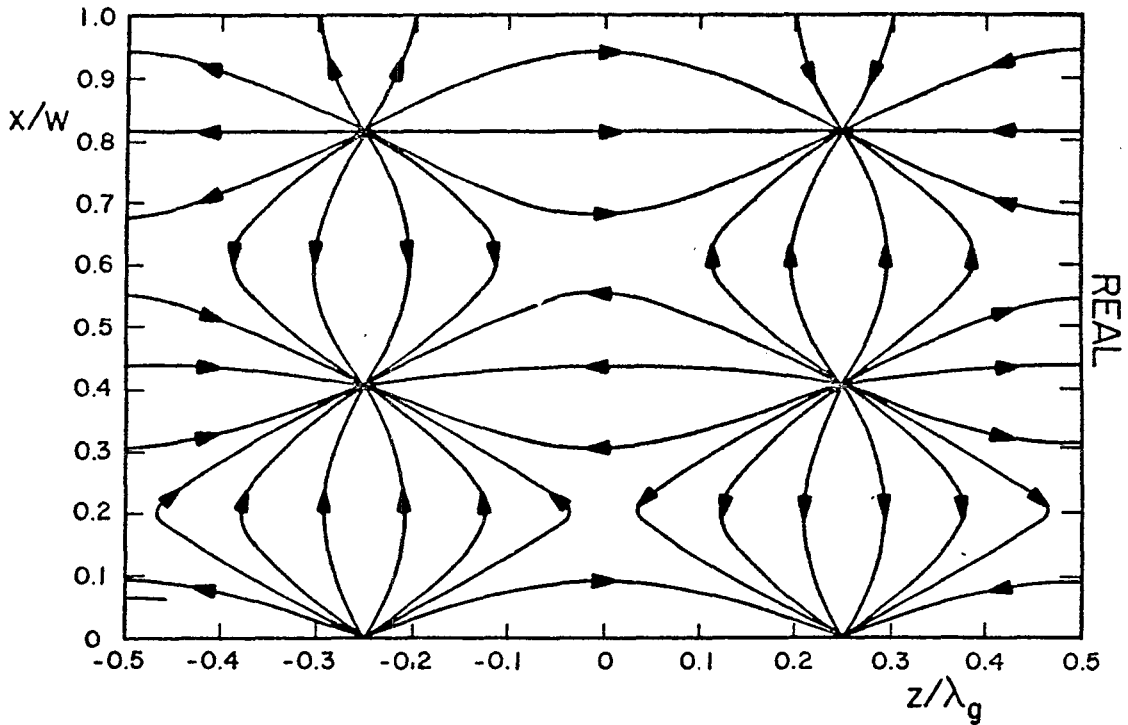
$$pw = -0.010 - i1.54, \quad kw = 4.46$$

Figure 12a. Field lines for the components tangential to the  $x, z$  plane of the magnetic field of the lowest odd antisymmetric TE mode.



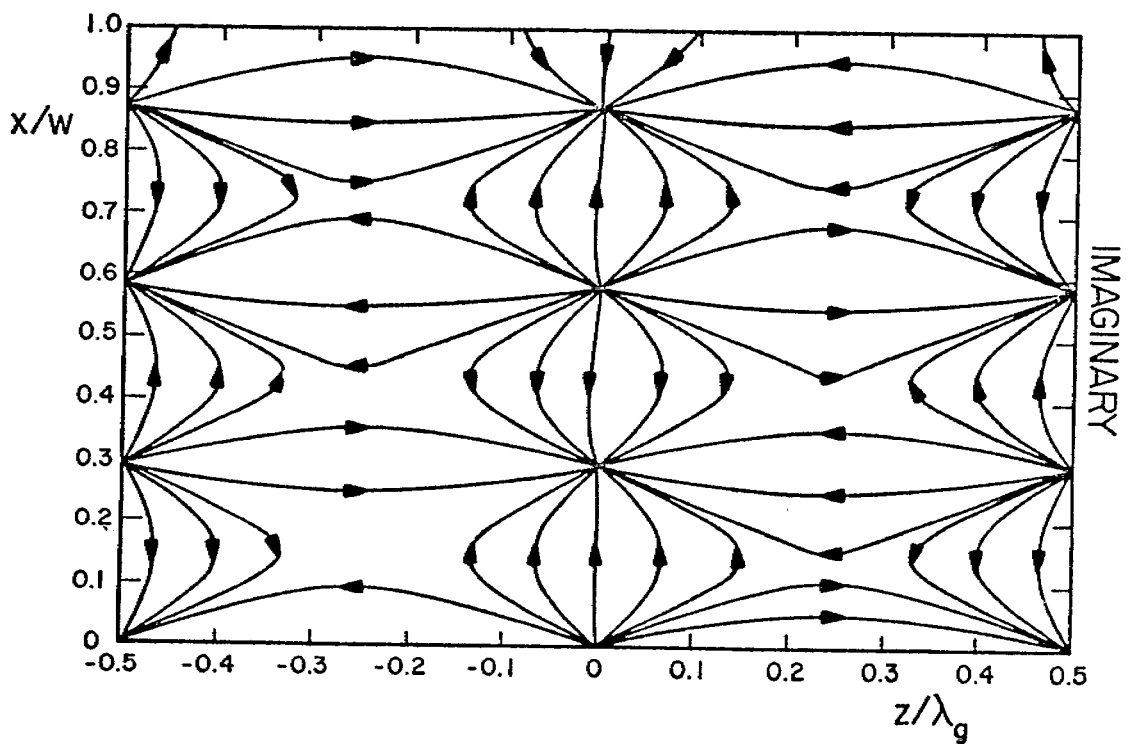
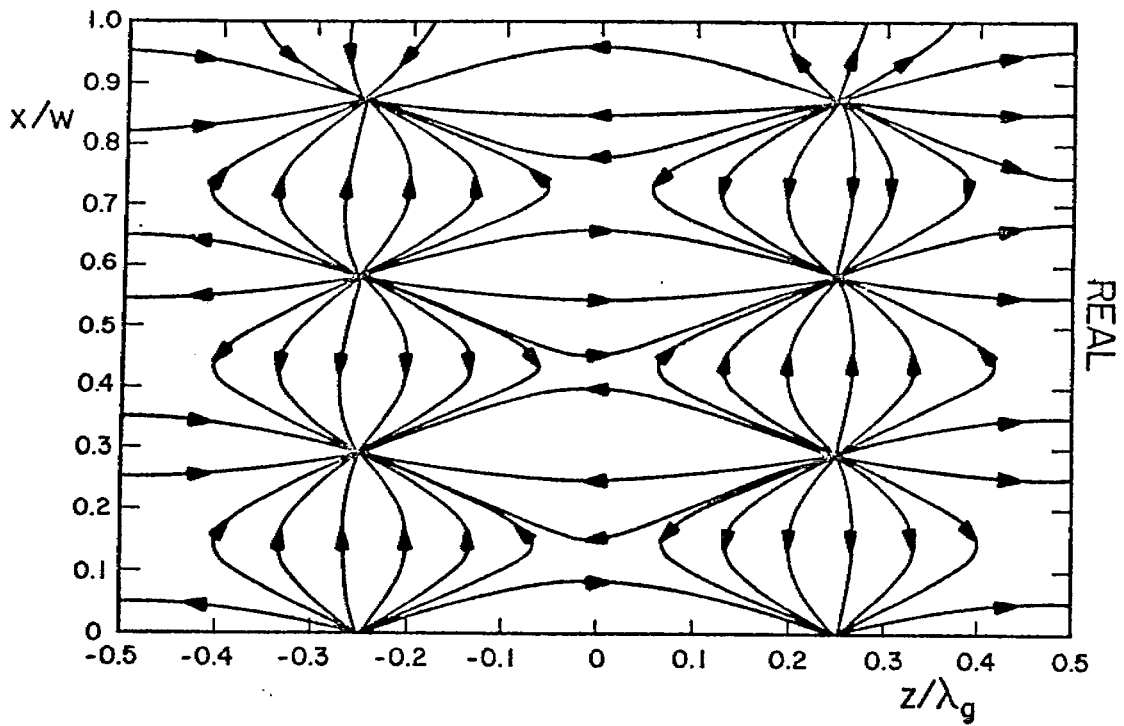
$$pw = -0.028 - i4.62, \quad kw = 6.24$$

Figure 12b. Field lines for the components tangential to the  $x,z$  plane of the magnetic field of the second lowest odd antisymmetric TE mode.



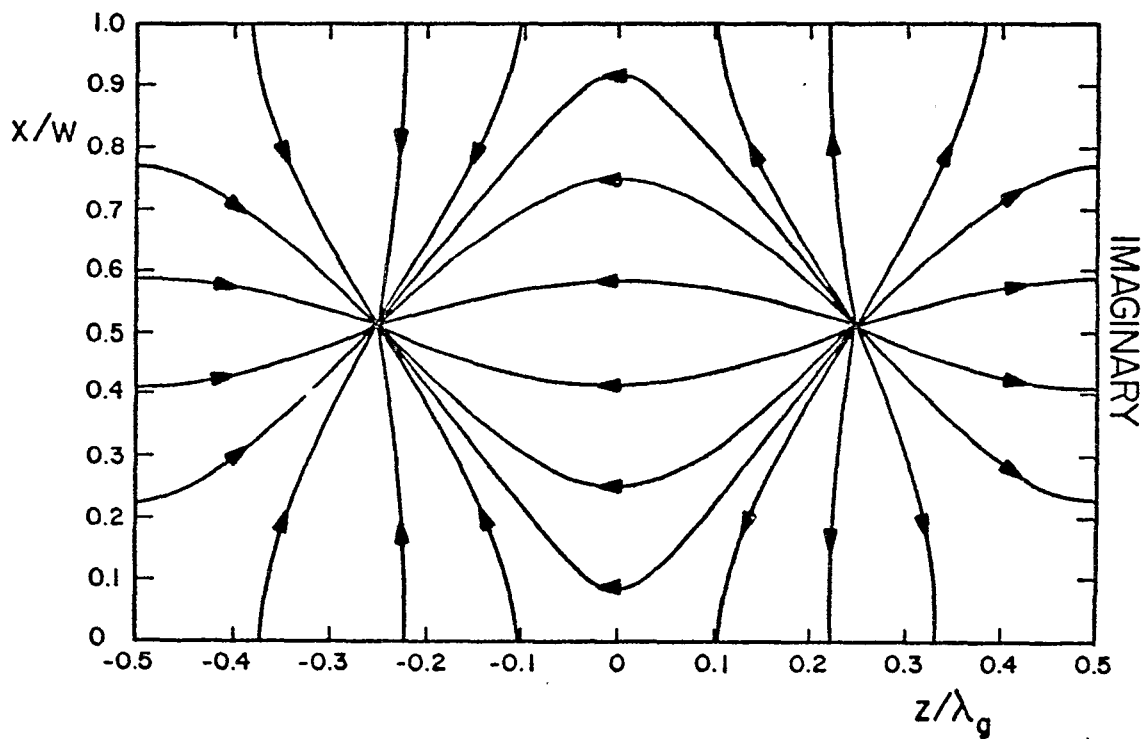
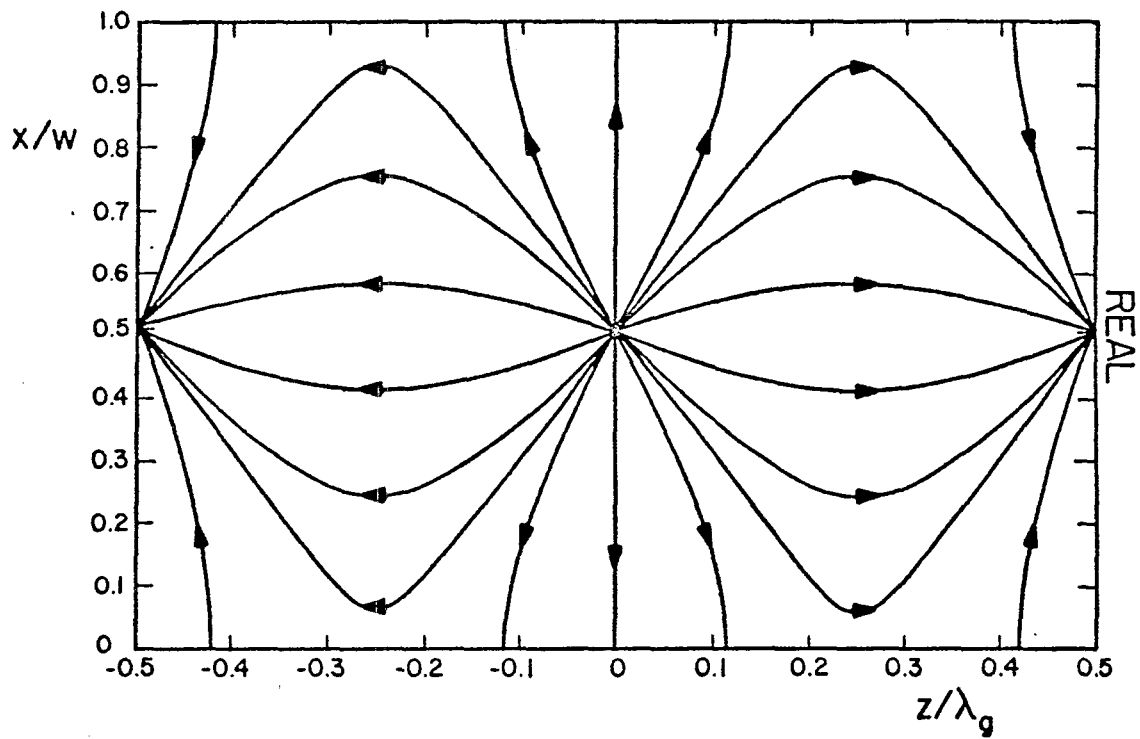
$$pw = -0.045 - i7.71, \quad kw = 8.77$$

Figure 12c. Field lines for the components tangential to the  $x, z$  plane of the magnetic field of the third lowest odd antisymmetric TE mode.



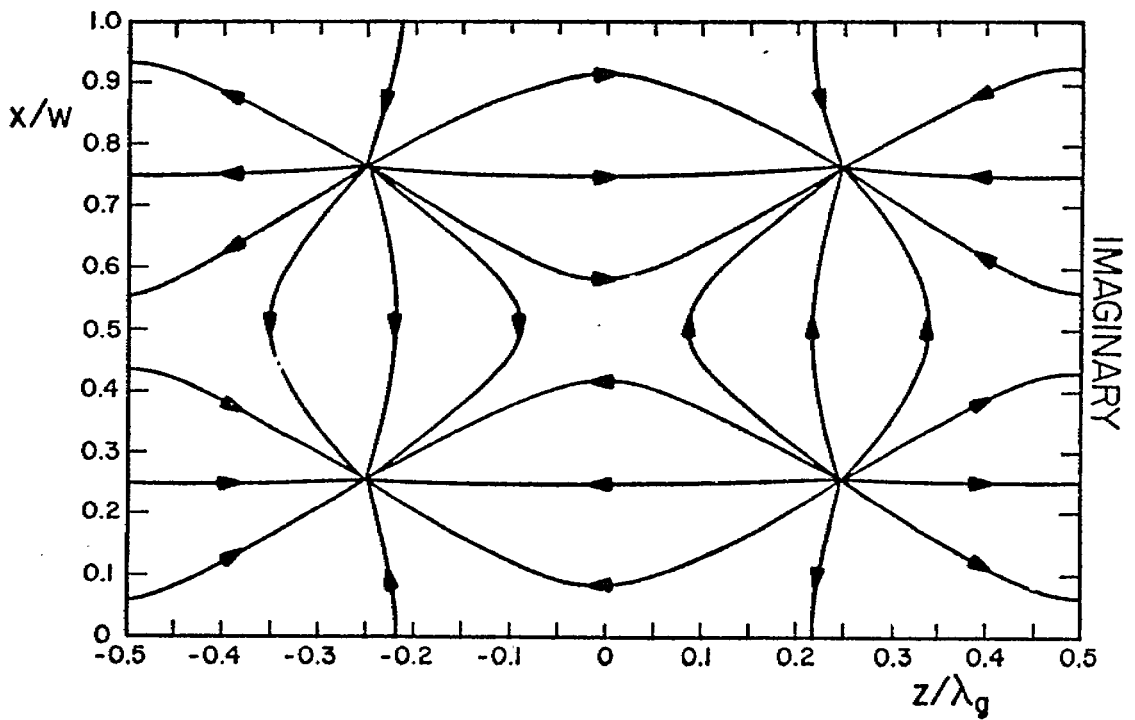
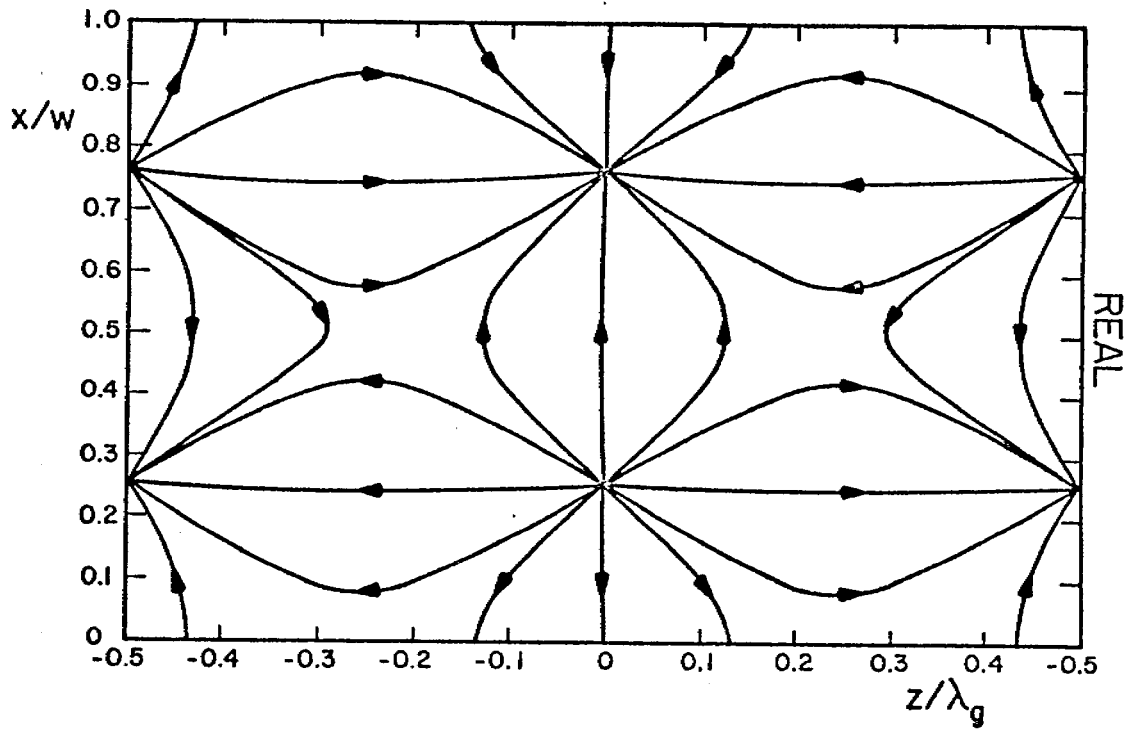
$$pw = -0.062 - i10.81, \quad kw = 11.59$$

Figure 12d. Field lines for the components tangential to the  $x,z$  plane of the magnetic field of the fourth lowest odd antisymmetric TE mode.



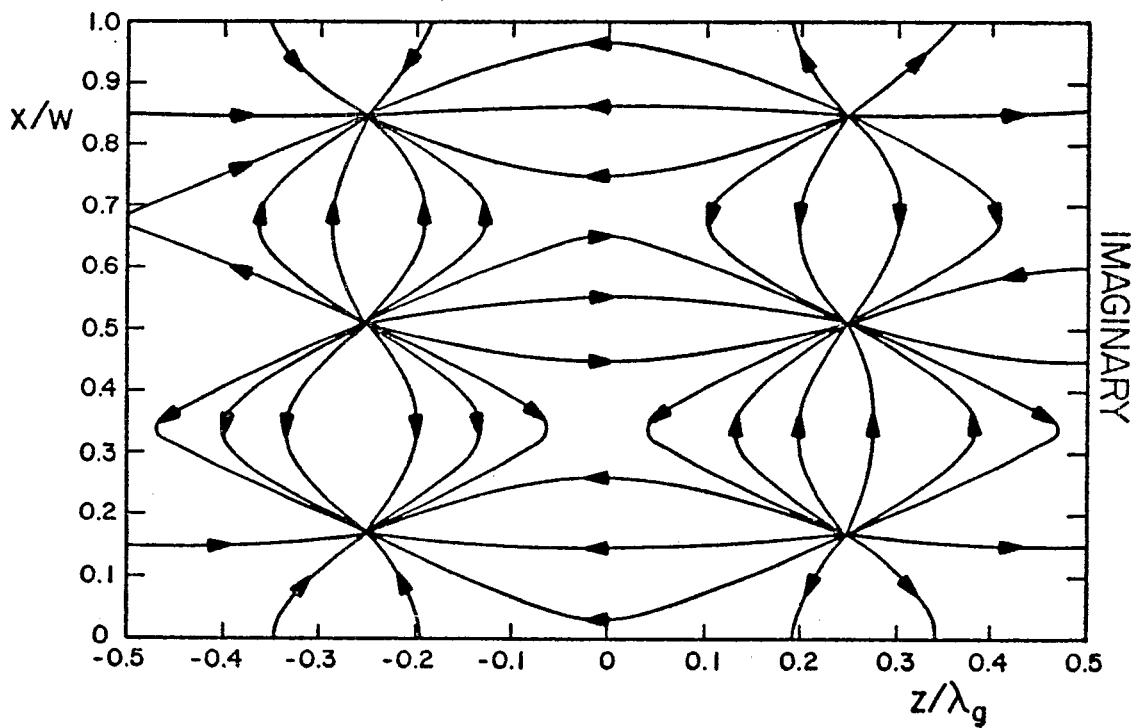
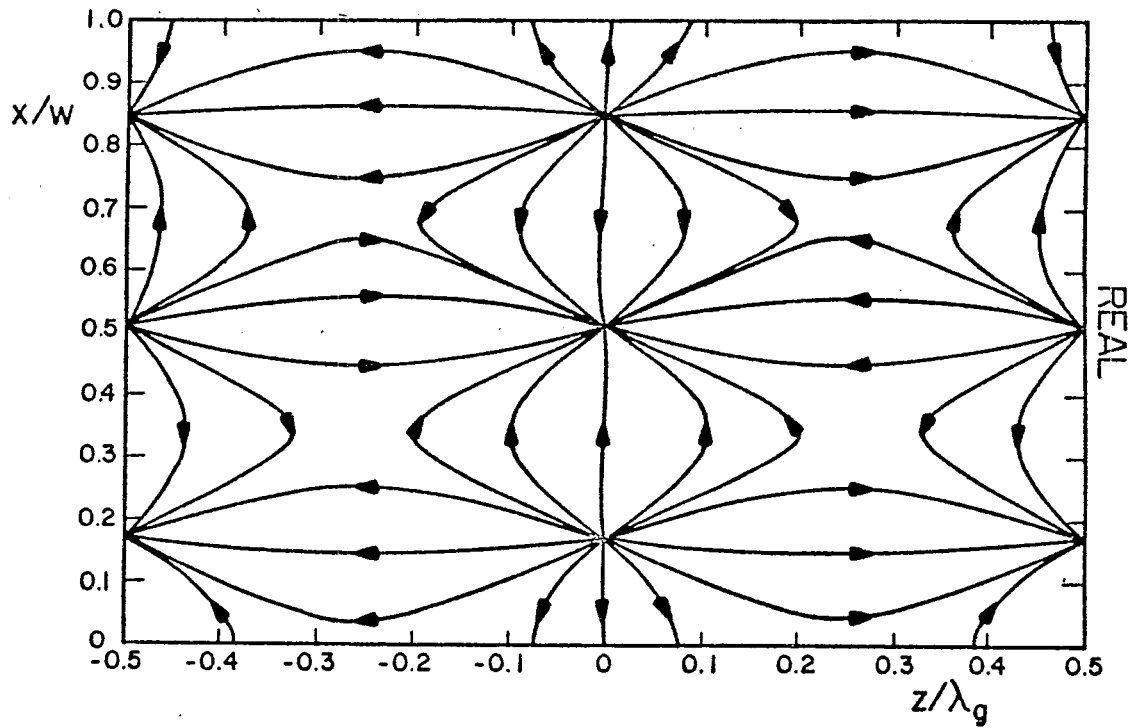
$$pw = -0.019 - i 3.08, \quad kw = 5.20$$

Figure 13a. Field lines for the components tangential to the  $x, z$  plane of the magnetic field of the lowest even antisymmetric TE mode.



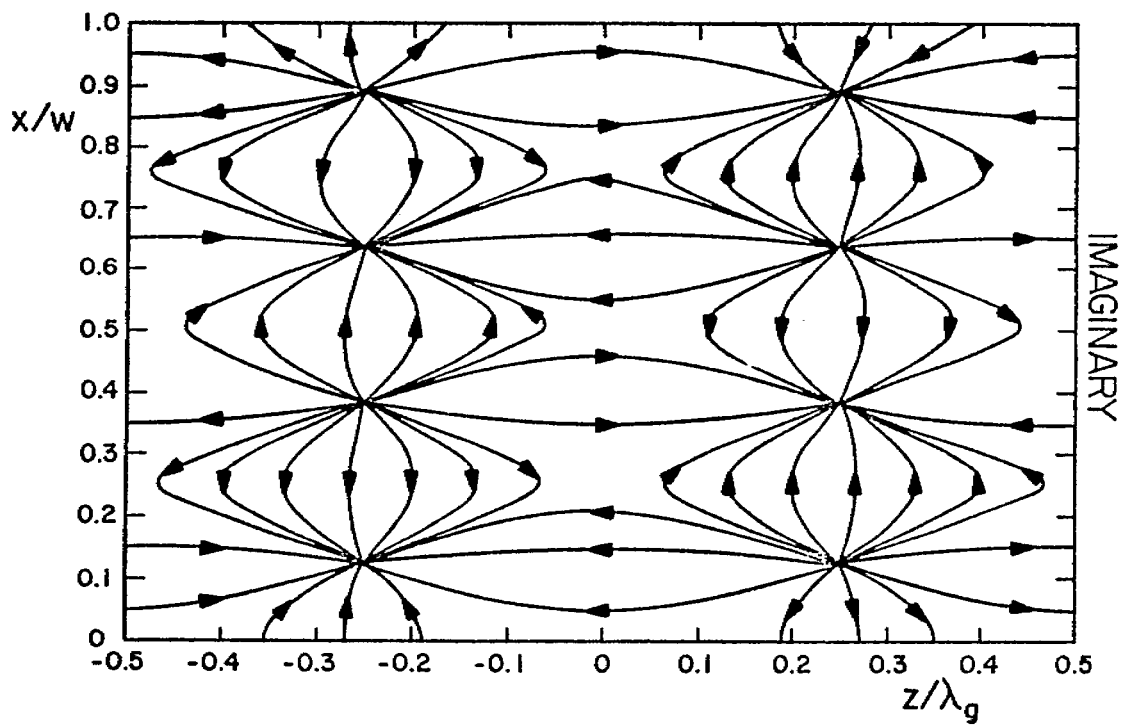
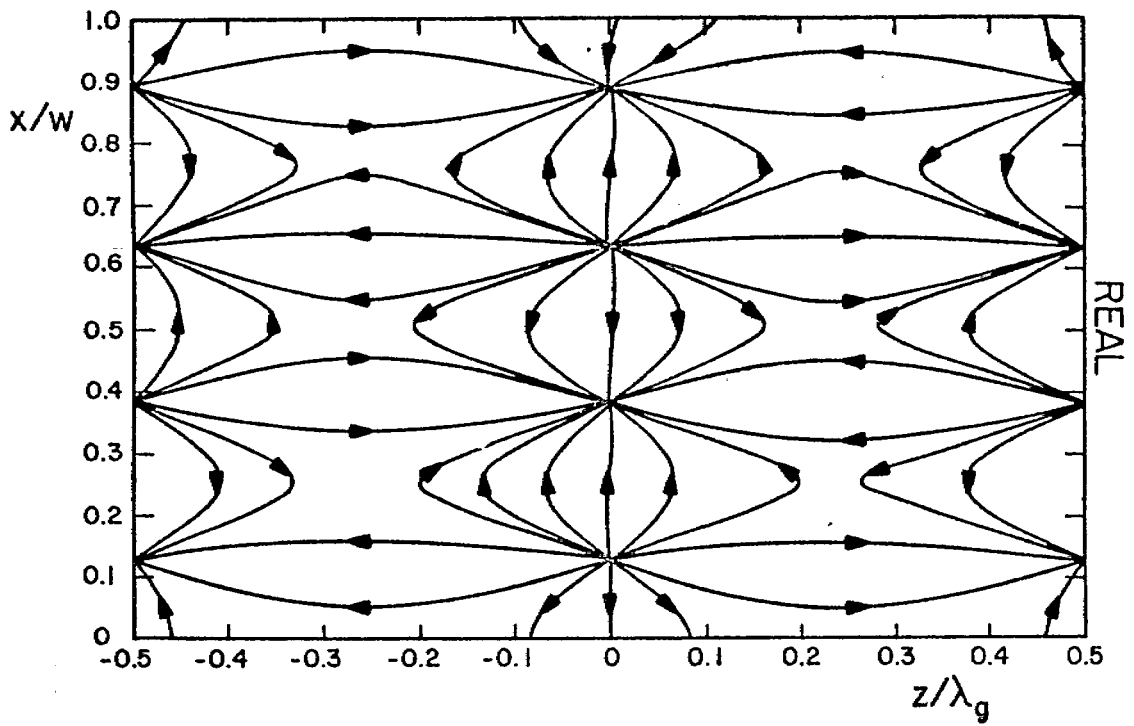
$$pw = -0.036 - i6.16, kw = 7.45$$

Figure 13b. Field lines for the components tangential to the  $x,z$  plane of the magnetic field of the second lowest even antisymmetric TE mode.



$$pw = -0.053 - i9.26, kw = 10.16$$

Figure 13c. Field lines for the components tangential to the  $x,z$  plane of the magnetic field of the third lowest even antisymmetric TE mode.



$$pw = -0.070 - i12.35, kw = 13.04$$

Figure 13d. Field lines for the components tangential to the  $x,z$  plane of the magnetic field of the fourth lowest even antisymmetric TE mode.

2. The divergence equation  $\nabla \cdot \underline{H} = 0$  implies that  $\nabla_t \cdot \underline{H}_t = -(\partial/\partial y)H_y$  where  $t$  denotes operations and components in the  $x, z$  plane. This latter equation shows that the (small)  $y$ -component can be viewed as a source function of the field tangent to the  $x, z$  plane.

The intensity of the field for a given mode can be indicated by the intensity of the field lines only if the magnetic field lines in the  $x, z$  plane are divergenceless in this plane. Since this is not the case for the considered  $H$ -field we can not use the density of field lines as a measure of the field strength. In fact, the vector plots show that the  $H$ -field is weak in regions of strongly concentrated field lines.

The field lines are constructed simply. An initial point  $(x_1, z_1)$  is chosen arbitrarily. The field is evaluated at  $(x_1, z_1)$ . A line segment of length  $\Delta$  is extended from  $(x_1, z_1)$  in the direction of the field at  $(x_1, z_1)$ . The new point  $(x_2, z_2)$  is located at the end of the completed line segment. The process is repeated, etc., and a mathematically smooth field line is formed.

## REFERENCES

- [1] C.E. Baum, "Impedance and Field Distributions for Parallel Plate Transmission Line Simulators," Sensor and Simulation Note 21, June 1966.
- [2] T.L. Brown and K.D. Granzow, "A Parameter Study of Two Parallel-Plate Transmission Line Simulators of EMP Sensor and Simulation Note 21," Sensor and Simulation Note 58, April 1968.
- [3] C.E. Baum, D.V. Giri, and R.D. Gonzalez, "Electromagnetic Field Distribution of the TEM Mode on a Symmetrical Two-Parallel-Plate Transmission Line," Sensor and Simulation Note 219, April 1976.
- [4] A.E.H. Love, "Source Electrostatic Distributions in Two Dimensions," Proc. London Math. Soc., Vol. 22, pp. 337-369, 1923.
- [5] L. Marin, "Modes on a Finite-Width, Parallel-Plate Simulator. I. Narrow Plates," Sensor and Simulation Note 201, September 1974.
- [6] L.A. Weinstein, Open Resonators and Open Waveguides, The Golden Press, Boulder, 1969.
- [7] T. Itoh and R. Mittra, "Analysis of Modes in a Finite-Width, Parallel-Plate Waveguide," Sensor and Simulation Note 208, January 1975.
- [8] L. Marin, "Modes on a Finite-Width, Parallel-Plate Simulator. II. Wide Plates," Sensor and Simulation Note 223, March 1977.
- [9] C.E. Baum, "Interaction of Electromagnetic Fields with an Object which has an Electromagnetic Symmetry Plane," Interaction Note 63, March 1971.